Torque Architecture For The Propulsion Supervisory Controller Of An Independent Axle All-Wheel Drive Electric Vehicle

Sopan Kane

Thesis submitted to the Faculty of the
Virginia Polytechnic Institute and State University
in partial fulfillment of the requirements for the degree of

Master of Science
in
Mechanical Engineering

Scott Huxtable, Chair
Steve Southward
Mehdi Ahmadian

August 30, 2024
Blacksburg, Virginia

Keywords: Torque Architecture, Electric Vehicles, Regenerative braking, Optimization, Energy Consumption, Vehicle Modeling

Torque Architecture For The Propulsion Supervisory Controller Of An Independent Axle All-Wheel Drive Electric Vehicle

Sopan Kane

(ABSTRACT)

This study describes the development of the Propulsion Supervisory Controller for an independent axle All-Wheel Drive Electric Vehicle, using a model-based approach. The vehicle has a main rear motor and a smaller front motor. Features like power moding, transmission range selection and torque architecture are discussed. For the torque architecture, different torque distribution strategies are explored in detail. Initially, a comparison of torque distribution strategies considering positive torques only, is used to assess the impact on the vehicle's energy consumption. Firstly, an optimal strategy with and without power-rate penalties is explored, which distributes the torque request to minimize the losses in both drive-units. Secondly, a fixed-ratio strategy is considered where both axles contribute with a predetermined torque ratio to meet the total torque demand. Thirdly, a torque-assist approach is examined, wherein only the rear motor contributes to the torque demand till it is operating at instantaneous maximum torque, after which the front motor starts contributing. Similar evaluations are then performed including regenerative braking or negative torque domain. Additionally, the performance of the penalized optimal strategy (PO) for positive torques is evaluated when combined with the torque assist regenerative braking strategy, where the front motor is primarily used for regenerative braking. The performance of PO combined with the ideal regenerative braking strategy is also assessed. This study aims to provide an overview of the controller development approach and an insight of the feasibility of deploying sophisticated computational algorithms for enhanced efficiency on it.

Torque Architecture For The Propulsion Supervisory Controller Of An Independent Axle All-Wheel Drive Electric Vehicle

Sopan Kane

(GENERAL AUDIENCE ABSTRACT)

This study focuses on the development of a propulsion controller for a modified all-electric 2023 Cadillac LYRIQ. The Sport Utility Vehicle (SUV) is equipped with a main rear motor and a smaller front motor. Functional features such as the power-up and power-down sequence and vehicle range selection are discussed along with performance features like torque control. The objective is to enable safe vehicle functionality and enhance the vehicle's powertrain efficiency through the development of software for its Propulsion Supervisory Controller (PSC). The study initially evaluates various strategies for distributing torque during forward acceleration. Three primary strategies are analyzed: an optimal approach aimed at minimizing overall energy losses, a fixed-ratio strategy where torque ratios are predetermined to meet the total demand, and a torque-assist method where the front motor provides torque only after the rear motor reaches its instantaneous maximum torque, triggered by the accelerator pedal input exceeding a threshold. Similarly, these strategies are examined within the context of regenerative braking to assess their impact on range. Finally, the penalized optimal torque distribution strategy is combined with a torque assist regenerative braking strategy as well as a strategy that adheres to the ideal braking distribution. This study provides an overview of the vehicle controller development and demonstrates the feasibility and benefits of employing advanced computational algorithms in the propulsion controller to achieve enhanced efficiency and an improved range in electric vehicles.

Dedication

I want to sincerely thank my family for their unwavering support and encouragement. I am also deeply grateful to Dr. Huxtable and Dr. Nelson for their continuous advice and feedback on this work and my involvement with HEVT. Their support has played a significant role in making me a better engineer.

I would like to extend my thanks to Dr. Ahmadian and Dr. Southward for their time in reviewing this work and for their guidance during the courses I took under their instruction.

Additionally, I would like to express my gratitude to the Department of Mechanical Engineering at Virginia Tech, EcoCAR EV Challenge sponsors and organizers, and all the HEVT members I have had the privilege to work with.

Acknowledgments

This work was partially funded by support from the U.S. Department of Energy EcoCAR EV Challenge, General Motors, and MathWorks Inc.

Contents

List of Figures ix

List of Tables xiii

1 Introduction 1

2 Literature Review 4

3 EcoCAR EV Challenge 8

3.1 Vehicle Development 8

3.1.1 Requirements 10

3.1.2 Modeling and feature development 11

3.1.3 Hardware-in-the-loop 12

3.1.4 Subsystem and System integration 12

3.1.5 Vehicle testing 13

3.1.6 Refinement 14

3.2 Powertrain Architecture Selection 14

3.2.1 Architecture 1 - eFAD and iDM-190 AWD 16

3.2.2 Architecture 2 - AAM RWD 19

3.2.3 Architecture 3 - dual iDM-190 AWD . . . 21
3.2.4 Architecture Selection Outcome . . . 24

4 Performance Modeling **26**

4.1 Reference Generator . . . 26
4.2 Longitudinal Driver . . . 27
4.3 Controller . . . 27
4.4 Vehicle Model . . . 28
4.4.1 Vehicle Body Model and wheels . . . 28
4.4.2 Drive unit model . . . 31
4.5 Model Validation . . . 33
4.5.1 Baseline model results . . . 33
4.5.2 Benchmarking a similar SUV (2021 Ford Mustang Mach-E RWD) . . . 39

5 Propulsion Controller logic **41**

5.1 Power moding . . . 41
5.2 Electronic Transmission Range Selection . . . 42
5.3 Torque architecture . . . 42

6 Torque Distribution Strategy **52**

6.1 Unpenalized Optimal Torque Distribution Strategy (UO) . . . 52
6.2 Penalized Optimal Torque Distribution Strategy (PO) . . . 56

6.3 Fixed-Ratio Strategy (FR) 57

6.4 Torque-Assist Strategy (TA) 58

6.5 Penalized Optimal Positive Torque combined with Ideal Regenerative Braking strategy (POIR) 59

6.6 Penalized Optimal Positive Torque combined with Torque-Assist Regenerative Braking strategy (POTA) 61

7 Simulation **62**

8 Results **67**

8.1 Performance - Positive torque (UDDS) 67

8.2 Performance - Including regenerative braking Torque (UDDS) 69

8.3 A comprehensive comparison between PO, and FR with and without regenerative braking for UDDS and HWFET 71

8.4 Performance evaluation of POIR and POTA 74

9 Discussion **77**

10 Conclusions **81**

List of Figures

3.1 System Engineering V-model 9

3.2 Architecture Selection Process 16

3.3 eFAD and iDM-190 AWD architecture 17

3.4 Architecture 1 - IVM to 60 mph time 17

3.5 Architecture 1 - 50-70 mph time 18

3.6 Architecture 1 - 60 to 0 mph braking distance 18

3.7 Single AAM motor RWD architecture 19

3.8 Architecture 2 - IVM to 60 mph time 20

3.9 Architecture 2 - 50 to 70 mph time 20

3.10 Architecture 2 - 60 to 0 mph braking distance 21

3.11 Dual iDM-190 AWD architecture 22

3.12 Architecture 3 - IVM to 60 mph time 22

3.13 architecture 3 - 50 to 70 mph time 23

3.14 Architecture 3 - 60 to 0 mph braking distance 23

3.15 Changing the stock 2023 RWD Cadillac LYRIQ architecture to the approved architecture for EcoCAR EV Challenge 25

4.1 Simplified MathWorks model 26

4.2 Vehicle body glider model 29

4.3 Interaction between vehicle and wheel model 31

4.4 Baseline LYRIQ Performance 33

4.5 Baseline model UDDS MPGe comparison 34

4.6 Baseline model HWFET MPGe comparison 35

4.7 Baseline testing - Vehicle velocity trace 36

4.8 Model validation - Motor Torque 36

4.9 Model validation - HV Battery Current 37

4.10 Model validation - HV Battery Voltage 37

4.11 Model validation - HV Battery State of Charge 38

4.12 Stock LYRIQ - IVM to 60 mph sensitivity analysis 38

4.13 2021 Ford Mustang Mach-E RWD Extended Range - 0 to 60 time 39

4.14 Mach-E UDDS MPGe comparison 40

4.15 Mach-E HWFET MPGe comparison 40

5.1 Power moding overview 41

5.2 ETRS overview 42

5.3 Torque architecture overview 43

5.4 Simplified full torque architecture logic 44

5.5 Accelerator Pedal-map 45

5.6 Torque speed envelope - front motor 45

5.7 Torque speed envelope - rear motor 46

5.8 Ideal total axle torque speed envelope 47

5.9 Simplified thermal derate strategy logic 48

5.10 Thermal derate strategy for front drive-unit 49

5.11 Thermal derate strategy for rear drive unit 49

5.12 Regenerative braking derating - SoC 50

5.13 Regenerative braking derating - speed 51

6.1 Optimal front contribution for positive axle torques 54

6.2 Optimal rear contribution for positive axle torques 54

6.3 Optimized front contribution, including regenerative braking torque 55

6.4 Optimized rear contribution, including regenerative braking torque 55

6.5 Ideal regenerative braking curve 60

7.1 Drive-trace validation for positive axle torques - UDDS 63

7.2 Torque traces for Positive Torques - UDDS 64

7.3 Torque traces for UDDS including regenerative torques 65

7.4 Torque traces for POIR and POTA - UDDS 66

8.1 UDDS Energy Consumption - Positive Torques 67

8.2 UDDS HV Battery SoC Time trace - Positive torques 69

8.3 UDDS Energy Consumption - Including regenerative braking Torque 70

8.4 UDDS HV Battery SoC Time trace - Including regenerative braking torques 71

8.5 UDDS energy consumption comparison between FR and PO with and without regenerative braking 72

8.6 HWFET energy consumption comparison between FR and PO with and without regenerative braking 73

8.7 UDDS Energy Consumption (kWh/100-miles for POIR and POTA) 75

8.8 HWFET Energy Consumption (kWh/100-miles for POIR and POTA) 76

List of Tables

3.1 Front drive unit specifications 24

3.2 Rear drive unit specifications 24

4.1 Comparison of model output with stock LYRIQ Vehicle Technical specifications 34

7.1 Simulation parameters 62

8.1 Summary of Energy Consumption results (UDDS) - Positive Torques 68

8.2 Summary of Energy Consumption results (UDDS) - including regenerative braking 70

8.3 Summary of comparison between PO and FR with and without regenerative braking (UDDS) 72

8.4 Summary of comparison between PO and FR with and without regenerative braking (HWFET) 73

8.5 Comparison of simulated combined adjusted range using FR, PO, POIR and POTA 76

List of Abbreviations

AWD All-Wheel Drive

BEV/EV Battery Electric Vehicle/Electric Vehicle

BMS Battery Management System

CAN Controller Area Network

CAVs Connected and Automated Vehicles

CSC CAVs Supervisory Controller

eFAD electric Front Axle Drive

EPA Environment Protection Agency

EPA Environmental Protection Agency

ETRS Electronic Transmission Range Selection

EVC EcoCAR EV Challenge

HEVT Hybrid Electric Vehicle Team

HIL Hardware-in-the-loop

HWFET Highway Fuel-Economy Test

I/O Input/Output

iDM integrated Drive Module

IVM Initial Vehicle Movement

LED Light-Emitting Diode

NCCP Normalized Cross Correlation Power

PI Proportional-Integral

PSC Propulsion Supervisory Controller

RWD Rear-Wheel Drive

SoC State-of-Charge

SUV Sports Utility Vehicle

TPIM Traction Power Inverter Module

UDDS Urban Dynamo-meter Driving Schedule

RWD vehicles are vehicles in which only the rear axle provides the driving torque

AWD vehicles are vehicles in which both, the front and the rear axles provide the driving torque

BEVs or EVs are vehicles that have pure electric powertrains, which usually consist of a high-voltage battery (for energy storage), inverters and different converters, traction motors, etc.

PSC is a controller that is responsible for various safety features (like isolation monitoring, relay control, etc.) and vehicle powertrain functionality features (like power moding, range selection, torque architecture, speed determination etc.). It receives messages from different vehicle controllers, CSC, drive units and hardware, processes these, and transmits these feature level messages to the relevant controller/hardware.

Battery Management System is a controller, which is responsible for ensuring that the high-voltage battery operates in a safe and efficient manner. It monitors different states like cell temperatures, voltages and current etc., and evaluates safe operating limits, state-of-charge, state-of-health etc. to transmit these to the application controller, in this case, the Propulsion Supervisory Controller.

CAVs refers to vehicles and vehicle systems, that can communicate with other vehicles, infrastructure and devices. These are usually associated with intelligent features like lane centering, adaptive cruise control, intersection navigation etc.

CSC is responsible for using sensor data for sensor fusion, to transmit CAVs critical signals to the PSC, other vehicle ECUs and hardware.

Hardware-in-the-loop testing refers to a testing strategy where the controller under test transmits and receives real-time messages to and from another real-time unit (test bench). The test-bench has the models/logic for the system controllers/hardware, and represents the system, which the controller will be deployed with.

EVC is an Advanced Vehicle Technology Competition, which is expected to run from 2022 to 2026.

IVM refers to the time-stamp when the vehicle traverses the first 1 foot in a launch event (starting from a reference of 0 feet).

Chapter 1

Introduction

The automotive industry is slowly transitioning to cleaner alternatives from conventional internal combustion engine vehicles. Sustainable mobility is being recognized as the need of the hour. When it comes to that, Battery Electric Vehicles (BEVs) come up as one of the viable options. The global EV market reached a total value of $ 500.28 billion in 2023 [13]. EVs used about 130 TWh of energy in 2023 [32]. Hence, with increasing adoption, there is scope for reducing energy consumption and increasing vehicle range in EVs.

There are multiple ways to reduce energy consumption in an EV. Reducing the mass of the body (as discussed in [7]) and rotational inertia of the rotating parts, and designing a more aerodynamic body, are a few. Using control strategies like efficient thermal management, regenerative braking, etc. could be a solution. Optimal selection and design of components like motors [11], transmission [31] etc. is another way. In the case of EVs with multi-motor powertrains, this can be achieved by developing an optimal torque architecture for the vehicle's longitudinal controller [9]. The torque architecture refers to the part of the logic in the vehicle's longitudinal controller or Propulsion Supervisory Controller (PSC) is responsible for allocating torque according to the instantaneous driver inputs as well as other vehicle states. This includes propulsion torque (or positive axle torque) in case of accelerator pedal inputs, as well as regenerative braking torque (or negative axle torque) while braking. Safety and efficiency are key aspects of this logic. For this paper, the vehicle under study is a 2023 Rear-Wheel Drive (RWD) Cadillac LYRIQ SUV. The original RWD

architecture of the vehicle is being modified into a dual-motor, all-wheel drive (AWD) architecture consisting of a main rear motor and a smaller front motor. This means that the vehicle's powertrain architecture is over actuated, and a torque split strategy is necessary. A MathWorks donated model [34] was modified to best represent the modified vehicle. The modification to the model included modeling the drive-units, and the modified vehicle-mass. Performance of torque split strategies exclusively for positive axle torques are first studied for evaluating energy consumption performance. Positive axle-torques refer to torques that are intended to accelerate the vehicle in the forward direction. Then, performance using full torque distribution strategies, i.e., including regenerative braking, are studied.

The Propulsion Supervisory Controller (PSC) is responsible for interpreting the vehicle's signals corresponding to the driver's intent as well as safety critical signals and using these to send torque commands to both the drive units (depending on the Power mode and Electronic Transmission Range Selection). The Propulsion Supervisory Controller is also responsible for the other vehicle level features like the vehicle startup/shutdown sequences, safety systems (High-Voltage isolation monitoring, Electronic Disconnect Switch etc.), Connected and Automated Vehicle systems (CAVs) Supervisory Controller (CSC) commands etc. For the torque architecture, specifically, in this case, the goal is to achieve the total wheel torque corresponding to the accelerator pedal position based on driver input, and instantaneous vehicle speed, efficiently and safely. The vehicle architecture under study is an overactuated system, because it has separate drive-units powering the front and the rear axles, with each drive unit consisting of an inverter having a local control system, for regulating current to the motors, to achieve the torque command. The control objective of the PSC is to evaluate the torque commands to the front and rear drive units based on the accelerator pedal position as well as the vehicle speed. This work provides a summary of the model-based development approach that HEVT is deploying for the development of the PSC software. Also, this work would be useful for evaluating whether it would be worth using a computationally heavier

torque distribution strategy, to improve vehicle range. The potential downside of that could be the controller not being able to handle other safety critical system signals and logic. Ultimately, Hardware-in-the-loop (HIL) testing, integration with the CAVs controller and in-vehicle testing of the Propulsion Supervisory Controller after the PSC logic is developed would be the next steps. Calibration using testing data for improving model fidelity and working with the drive-unit manufacturers to improve safety and performance, would be necessary.

Chapter 2

Literature Review

The V-model of Systems Engineering [10] has closely been followed throughout the project. Understanding the V-model is key to being able to develop and test powertrain features to ensure that the features are safe and efficient. Continuous verification at all stages including Model-in-the-Loop, Hardware-in-the-loop and Vehicle-in-the-loop is crucial.

Modeling and model-in-the-loop testing is one of the first and most crucial steps in EV Propulsion Controller development. In [4], a MATLAB/Simulink model is built and simultaneously tested against dynamometer results. An accurate model of the EV Propulsion Controller, can be used for defining vehicle technical specifications like acceleration, range, braking distance etc. These can then be used to verify that the vehicle would be a good market fit and hence, also meet customer facing specification targets potentially derived from market research. Control strategies can also be tested in the simulation and modeling environment.

An accurate model can also be crucial, to move to the next phase of the V-model with HIL testing. [19] demonstrates a systematic approach to take propulsion controller logic from model to algorithm to real-time implementation. [8] describes modeling methods, keeping model-based HIL testing in mind. HIL testing is crucial even from a systems safety standpoint. [38] describes development of a Hybrid Electric Vehicle controller implementing a model-based development approach keeping systems safety in mind. A hybrid mode selection function considering functional safety from the standpoint of the battery is also

discussed. Battery temperature and state-of-charge are considered as the key parameters for the drive mode selection. A fault insertion approach is used in HIL to ensure that the controller responds correctly. Another key observation is that, as opposed to HEVs, BEVs have the capability to instantaneously change torque commands to the electric machines and there is no real need to implement delays. In EVs, there are other parameters like BMS limits (Voltage, Current and Power), motor temperatures, errors and fault statuses (like HV battery isolation monitoring, sensor faults etc.) that need to be considered. The study also describes the importance of model validation and accuracy of the plant model when following a model-based approach.

Vehicle level validation comes next in the V-model. Vehicle systems are usually tested using predefined drive-cycles. But the life and performance of vehicle systems would vary greatly in the case of real-world application. [5] describes how real-world application of Lithium-ion batteries can impact the range of the electric vehicles, by reducing the capacity of the battery and increasing the internal resistances (which increases the energy consumption). Data from testing vehicles or vehicle systems in real-world can be used for improving model fidelity and refinement. The validation is conducted keeping in mind the higher levels of requirements (mostly the vehicle technical specifications).

EV Architecture selection is one of the key factors that influences the rest of the vehicle development process. Depending on the type and configuration of the powertrain hardware, the software on the controller can then be designed. Various types of configurations and types are explored in [39]. Then, various parameters like efficiency, weight, cost etc. of different types of motors are studied. The effect of the type of architecture on energy consumption has been explored in [35].

In a model-based approach, a model of the complete system is the focal point, for the powertrain and vehicle development. The model is used and updated in all phases of the V-model. Starting from feasibility analysis, simulation, and goal setting followed by requirement/specification definition, system and sub-system level feature development, verification and validation, and real-time implementation, the model is constantly refined and utilized. A methodology on how to implement model-based development, by continuously refining and correcting the model, is discussed in [22].

For multi-motor vehicle architectures, there is a possibility of relatively improving the range by using optimal methods for torque distribution. This can be done by ensuring that the drive-units operate in the best efficiency regions.

A comparison of an optimal torque distribution strategy with the average distribution method was done by Na et al. [27] and Yuan et al. [41]. A comparison of optimal torque-distribution strategy with a non-linear model predictive control strategy and a fixed ratio strategy was also discussed in [40]. The optimal control strategy discussed in these studies does not consider the rate at which power transmitted can change between each simulation time step. These studies also do not consider gearbox losses. Independently driven electric vehicle configurations with 4 drive units were explored by Wang et al. [36] and Liang et al. [24]. [36] uses an optimal torque distribution strategy to minimize energy consumption, and then, a particle swarm optimization to support powertrain component selection decisions. A torque allocation strategy to minimize energy consumption, while enhancing handling performance, has been discussed in [24].

With regard to regenerative braking, brake blending becomes important. A regenerative

braking strategy maximizing energy recuperation, while considering a fore-aft brake distribution for a hybrid vehicle, is discussed in [15]. [42] describes a regenerative braking control strategy for a mining truck (all-wheel drive, with a front and rear drive unit), which first splits torque between friction and regenerative braking and then the regenerative torque, between the front and the rear drive units. Road slope is also considered. A regenerative braking model for brake blending, based on brake pedal position and an axle lock-up prevention algorithm, has been discussed in [29].

Overall, it is useful to evaluate the effectiveness of using sophisticated algorithms in improving the range of EVs.

Chapter 3

EcoCAR EV Challenge

The EcoCAR EV Challenge (EVC) is a 4-year student competition [3]. US Department of Energy Argonne National Laboratories (ANL), General Motors (GM) and MathWorks are the title sponsors for the competition. The competition is split into 4 phases:

1. Design
2. Build, and Integrate
3. Test
4. Refine

The current work was completed during Year 1 and Year 2 of the EcoCAR EV Challenge. Virginia Tech's EcoCAR team HEVT, is taking part in the competition, with the main goals of integrating an Advanced Propulsion System, with Connected and Automated Vehicles (CAVs) technology, focusing on Energy Efficiency and Systems Safety, Consumer Appeal and Equity in Mobility, specifically in EV SUV domain.

3.1 Vehicle Development

The team follows a system V-model for the vehicle development process. The workflow is a modified version of the [33]. [25] also describes the model-based vehicle development process

for a hybrid-electric vehicle.

Hence, in this study, the V-model has been tailored to best fit the needs of HEVT's Propulsion Controls and Modeling team for the EcoCAR EV Challenge. A visualization of the V-model that is being utilized by HEVT is shown in Figure. 3.1. It is important to keep in

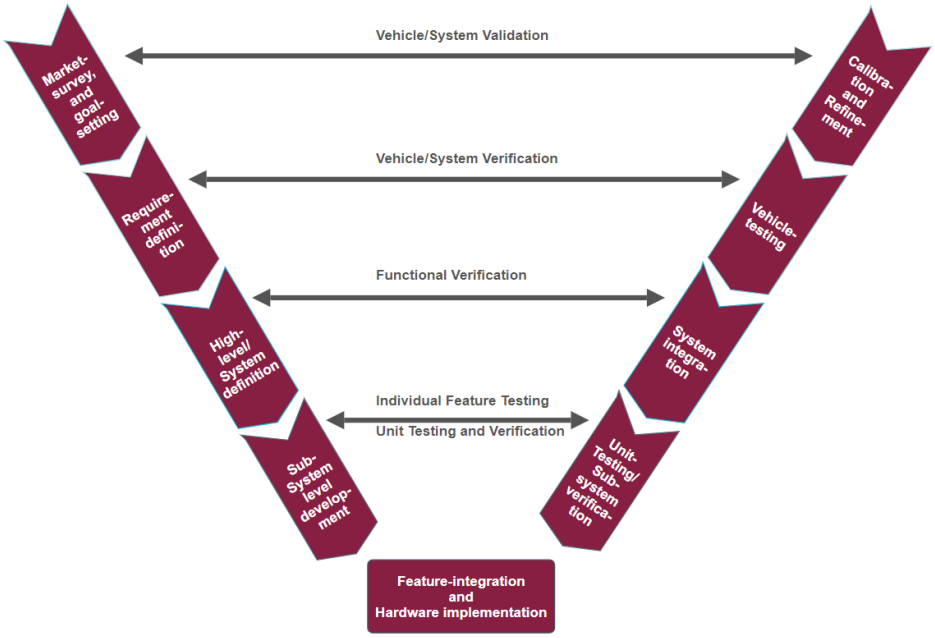

Figure 3.1: System Engineering V-model

mind that the team is integrating drive units and components manufactured by OEMs other than GM, with a GM vehicle. Hence, the controller being developed is responsible for facilitating the communication between the vehicle Electronic Control Units i.e. ECUs (which handle all driver inputs), the CAVs Supervisory Controller i.e., CSC (which handles all the autonomy related signals), drive-unit signals (which are responsible for torque commands etc.) and other team added hardware (like LEDs, displays, systems safety hardware etc.). It is also important to note that the TPIM (Traction Power Inverter Module) of the stock LYRIQ drive unit, is responsible for transmitting a lot of other signals like the vehicle speed feedback, actual transmission range, drive-unit temperature etc. Hence, because the TPIM

is being removed, it is important that the PSC receives the critical signals from the team added components, processes them and correctly transmits signals that the vehicle ECUs are expecting, that would otherwise be transmitted by the stock TPIM on the relevant CAN bus.

3.1.1 Requirements

Starting with requirements, the team developed its own set of system requirements based on the following:

1. Software and Systems Safety
2. Hardware
3. Performance

1) Software and Systems Safety requirements: The software requirements were mainly centered around Propulsion Controls features. These would be utilized in Year 1 and Year 2. The main features include:

- Power moding and contactor control: To enable and disable the Propulsion System safely, based on driver inputs.
- Electronic Transmission Range Selection and Vehicle immobilization: To communicate the driver requested range to the drive units.
- Torque and speed: This includes vehicle speed determination, as well as the torque architecture, which will be discussed in depth in this paper.

- Some other features include CAVs features (like eco adaptive cruise control, cybersecurity and authentication etc.). There are also other systems safety features like the electronic disconnect switch to manually control the HV bus contactors, ground-fault detection and warning, etc.

2) Hardware requirements: These are mainly centered around the wiring connections and communication protocols (CAN, analog and digital I/O) between the vehicle controllers, drive-unit inverters/motor controllers, CSC and other team added hardware (e.g., isolation monitoring device, low voltage power distribution system, electronic disconnect switch etc.). These would be utilized in Year 2 and Year 3.
3) Performance requirements: These are based on results from the architecture selection and the goals that were set. The integrated vehicle would be tested to ensure that each of these requirements, corresponding to team vehicle technical specification target, is met. These requirements would be used in Year 3 and Year 4 in the testing and refinement phases.

3.1.2 Modeling and feature development

Based on requirements, modeling and simulation were completed. Firstly, the base model was validated. Then the base model was modified to best represent the team vehicle. Then, a model-based development approach was followed. This yielded all features to be implemented on the vehicle. As an example, the vehicle model was used to compare performance of different torque distribution strategies based on energy consumption.

3.1.3 Hardware-in-the-loop

A Speedgoat Performance real-time unit was used as the HIL-test bench. The PSC itself is a Speedgoat Baseline M real-time unit. HEVT used a combination of a model-based approach and a signal replay approach to validate the PSC logic on HIL. Soft ECUs were modeled and run on the HIL bench, whereas the PSC logic was run on the PSC. The model-based approach comprised of modeling sub-systems on the HIL bench to replicate the vehicle controllers. These are called soft ECUs. For the replay approach, HEVT logged Baseline data from the vehicle and replayed relevant signals. Test cases were used to test various scenarios like start-up and shutdown sequence of the vehicle to test the power moding logic.

3.1.4 Subsystem and System integration

This would include testing and validating the logic on the PSC with actual hardware and real-time vehicle signals. As an example, for testing the ETRS, the PSC would be connected to the relevant vehicle CAN bus. The driver would then shift the ETRS lever. Then, verifying that the correct transmission messages are transmitted by the PSC would complete the subsystem integration and validation for the ETRS feature. Also, a lot of Propulsion System features depend on each other. For example, ETRS requires that the Propulsion System is active, to send the correct transmission messages. Hence, full system integration and validation is critical. This includes testing the complete logic in the PSC and its interaction with the vehicle, CSC, drive-units and other hardware.

3.1.5 Vehicle testing

Vehicle testing includes a series of tests to verify that the PSC is correctly integrated with the vehicle. HEVT split the test plan into test-legs

1. Systems safety testing: These tests evaluate systems safety component functionality. These include HV tests (like HV isolation monitoring, EDS and relay control, etc.).
2. Functionality testing: These tests validate that the system functionality software is correctly integrated. Testing the start-up and shutdown sequences, ETRS functionality etc.
3. Performance testing: IVM to 60 mph time, 50 to 70 mph time, braking distance. tip in and tip out, etc.
4. Energy consumption testing: Team developed city drive cycle energy consumption, team developed highway drive cycle energy consumption, coast down tests etc.
5. CAVs tests: Adaptive Cruise Control, Automatic intersection navigation, Auto park test, Lane-centering control etc.
6. Calibration tests: Tip-in tip-out tests, Part-load acceleration, etc.

Test legs consist of test-cases. Each test-case has the following information.

1. Test description/summary.
2. Required signals.
3. Detailed procedure.
4. Post-processing requirements.
5. Passing criteria.

3.1.6 Refinement

In the refinement phase, the feedback from the full vehicle test can be used to further improve the subsystems and features to be able to bring the test-results closer to the target.

3.2 Powertrain Architecture Selection

During Year 1 of the competition, teams had to go through the process of selecting drive-units and configuration for finalizing the powertrain architecture. Please note that the term drive-unit refers to a motor-inverter-gearbox system or unit. The baseline model was modified to best represent the architecture being modeled (including the configuration, i.e., AWD or RWD and drive-units being used). Different possible architectures were modeled. Then, vehicle performance, including acceleration, braking and energy consumption were evaluated. HEVT finalized 3 architectures, out of which, one was approved. The following parameters are evaluated for each architecture under study.

1. Acceleration:

    - IVM to 60 mph: In this test-case, the vehicle starts at 0 mph and is accelerated to 90 mph. The time elapsed between when the vehicle rolls out by 1 foot and when the vehicle speed reaches 60 mph is the IVM to 60 mph time. A 0-to-90 mph step reference velocity is used as an input and the output i.e., actual velocity of the vehicle model is logged. This is done to ensure the best effort acceleration. The 0-to-60 time simply refers to the time elapsed between when the accelerator pedal is pressed to its 100% position for the test and the vehicle reaching 60 mph. For calculating the IVM to 60 speeds, the IVM time had to be calculated. IVM time refers to the time that the vehicle takes to move forward by 1 foot, when

using its best effort (i.e., for a 100% accelerator pedal position). The time taken for the integral of the vehicle speed to reach 1 foot is the IVM time. The time elapsed between the vehicle moving forward by 1 foot and reaching 60 mph refers to the IVM-to-60 time. For this study, the accelerator pedal is pressed to 100% at approximately 20 seconds of simulation time.

- 50 to 70 mph: A custom drive-trace is set up for this test-case. A reference speed starting at 60 mph, transitioning into a cruising 50 mph, and then accelerating to 90 mph (again, to ensure the best effort acceleration) is used as the input. This corresponds to GM's standard testing procedure. The time that the vehicle model takes to get from 50-to-70 mph is then recorded. For this study, the deceleration from 60-to-50 mph is at 40 seconds of simulation time and the accelerator pedal is pressed to 100% at 80 seconds of simulation time.

2. Braking distance (60 to 0 mph): A reference speed starting at 60 mph and then dropping to 0 mph at 40 seconds of simulation time, is given as the input to the model. This corresponds to the vehicle cruising at 60 mph and suddenly braking with a 100 % brake pedal position (i.e., best effort deceleration). The vehicle model's actual speed was used to calculate the braking distance. For calculating the braking distance, the speed was integrated with respect to time, for the time between when the brake pedal was pressed to a 100% position and when the vehicle comes to a stop.

3. Range (Combined).

A simplified flow-diagram of the architecture selection process is shown in Figure 3.2.
The model outputs were first used for comparison of the architecture being proposed with similar SUVs in the market. Model outputs were also used to check that the vehicle complies with the performance related vehicle design rules (minimum range, maximum IVM-60 mph

time, maximum braking distance etc.). Then, external and non-quantitative parameters like ease of integration, technical support from drive-unit manufacturers, timeline for procurement, cost etc. can be integrated, by assigning weights to these parameters.

The architecture selection was based on a risk assessment using a trade-off matrix.

The trade-off matrix was generated as follows. Common risk cases were identified, and an RPN number (based on probability of occurrence, severity of risk case and ease of detection of risk case) assigned to each risk case within each architecture. Then, totaling these for each architecture, the architecture with the minimum risk was chosen as the team-preferred architecture.

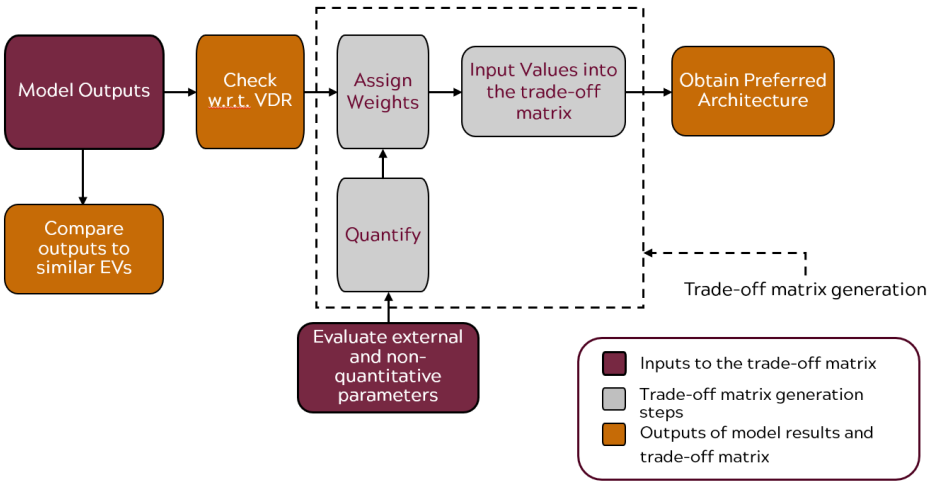

Figure 3.2: Architecture Selection Process

3.2.1 Architecture 1 - eFAD and iDM-190 AWD

This was the medium performance, medium energy consumption architecture proposed by VT. It has a 50-kW electric Front Axle Drive-unit (eFAD), and a 182 kW (350 V Nominal Voltage) Cascadia iDM-190 rear drive unit. The front motor has a peak torque of 150 N and a transmission ratio of 10.08 and the rear motor has a peak torque of around 500 N and a

transmission ratio of 8.28. Architecture -1 is shown in Figure 3.3. The performance plots of architecture 1 can be seen in Figures 3.4, 3.5 and 3.6.

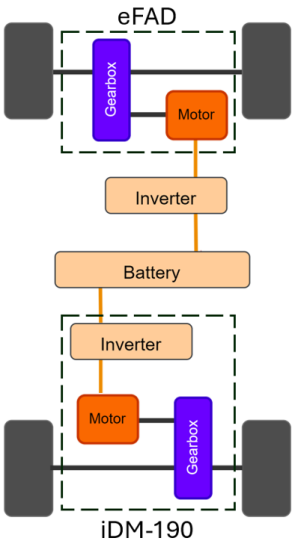

Figure 3.3: eFAD and iDM-190 AWD architecture

The simulated IVM to 60 mph time for architecture 1 is 6s

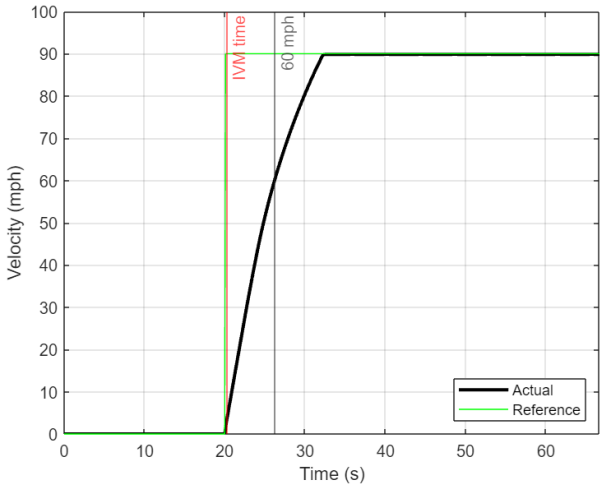

Figure 3.4: Architecture 1 - IVM to 60 mph time

The simulated 50 to 70 mph time for architecture 1 is 3.2 seconds

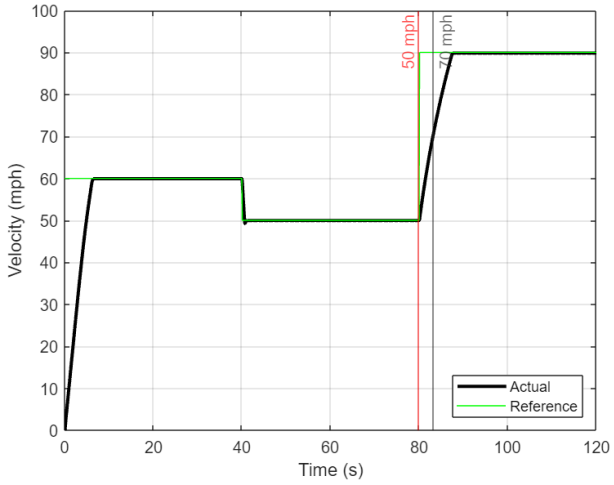

Figure 3.5: Architecture 1 - 50-70 mph time

The simulated braking distance for architecture 1 is 45.22 m.

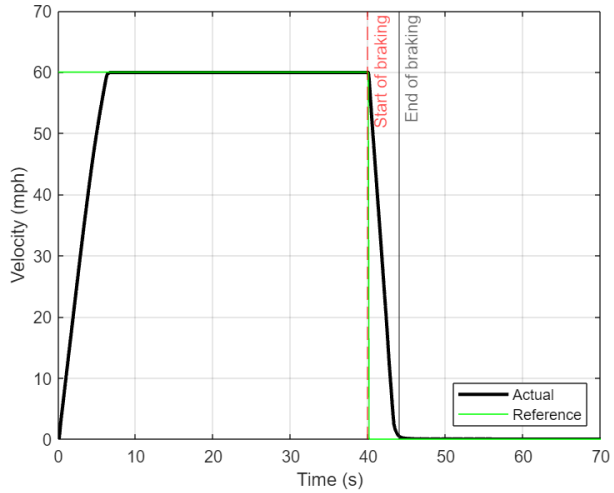

Figure 3.6: Architecture 1 - 60 to 0 mph braking distance

The simulated adjusted combined range for the architecture 1 is 262 miles.

3.2.2 Architecture 2 - AAM RWD

Architecture 2 is the low performance, low energy consumption architecture proposed by VT. It has a 225-kW rear drive unit with a peak motor torque of 225 Nm and a transmission ratio of 18:1. Architecture 2 is shown in Figure 3.7. The performance plots for Architecture 2 are shown in Figures 3.8, 3.9 and 3.10.

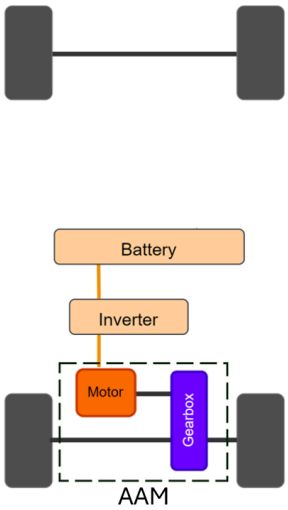

Figure 3.7: Single AAM motor RWD architecture

The simulated IVM to 60 mph time for architecture 2 is 8.1s

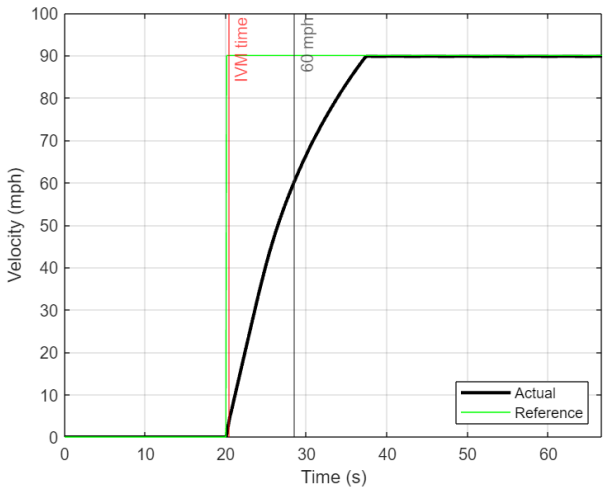

Figure 3.8: Architecture 2 - IVM to 60 mph time

The simulated 50 to 70 mph time for architecture 2 is 4.5s

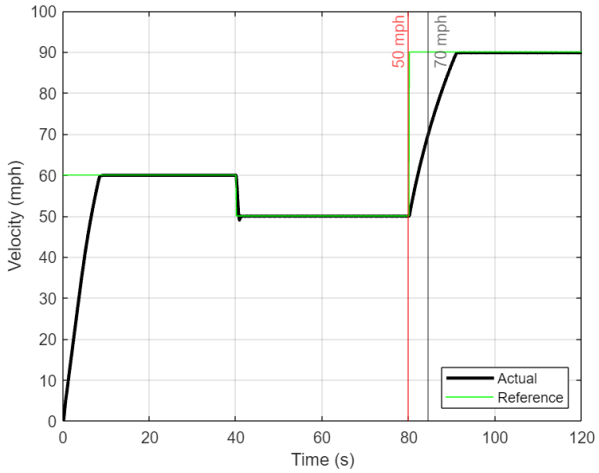

Figure 3.9: Architecture 2 - 50 to 70 mph time

The simulated braking distance for architecture 2 is 47.25 m

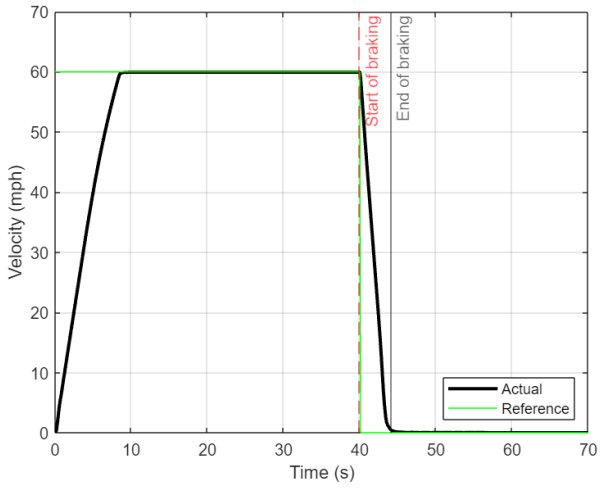

Figure 3.10: Architecture 2 - 60 to 0 mph braking distance

The simulated adjusted combined range for architecture 2 is 268 miles.

3.2.3 Architecture 3 - dual iDM-190 AWD

This was the high-performance, high energy consumption architecture proposed by VT. It has one 210 kW iDM-190 drive unit on each axle (front and rear). Architecture 3 is shown in Figure 3.11. The performance plots for architecture 3 are shown in Figures 3.12, 3.13, and 3.14.

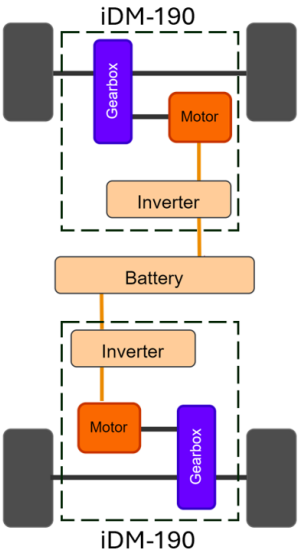

Figure 3.11: Dual iDM-190 AWD architecture

The simulated IVM to 60 mph time for architecture 3 is 3.8s.

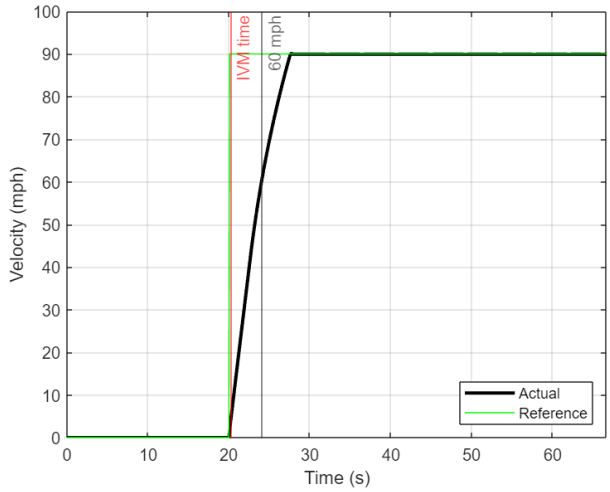

Figure 3.12: Architecture 3 - IVM to 60 mph time

The simulated 50 to 70 mph time for architecture 3 is 2s

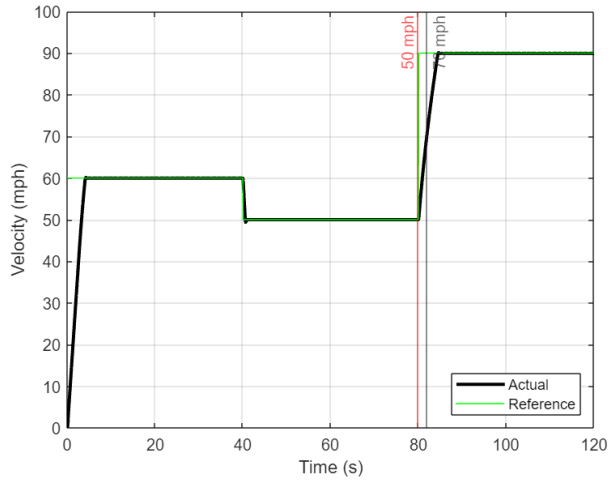

Figure 3.13: architecture 3 - 50 to 70 mph time

The simulated braking distance for architecture 3 is 41.4

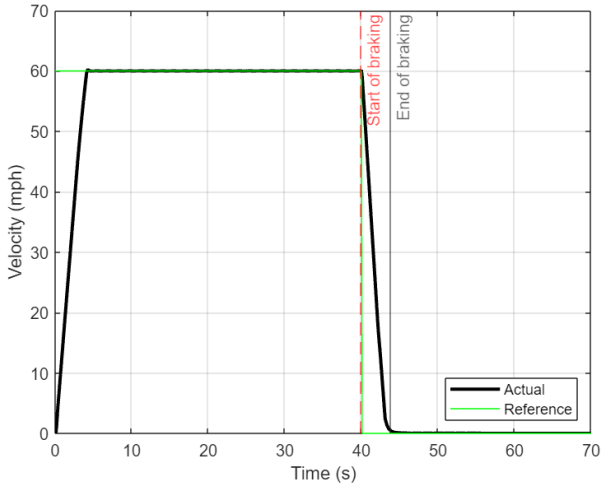

Figure 3.14: Architecture 3 - 60 to 0 mph braking distance

The simulated adjusted combined range for this architecture is 253 miles.

3.2.4 Architecture Selection Outcome

Architecture 1 is the team preferred architecture, which has been approved by the competition. Hence, the goal for Year 2 of the competition has been to replace the stock RWD configuration of the 2023 Cadillac LYRIQ with a dual-motor AWD architecture corresponding to Architecture 1. Tables 3.1 and 3.2 show the specifications of the front and the rear drive-unit. Figure 3.15 shows the overall goal for HEVT for Year 2 of the EcoCAR EV Challenge.

Table 3.1: Front drive unit specifications

Electric Front Axle Drive (eFAD)	
Transmission (G_{front})	10.08:1
Peak Power	50 kW
Peak Motor Torque ($T_{cap-front}$)	150 Nm

Table 3.2: Rear drive unit specifications

Cascadia Integrated Drive Module 190 (iDM-190)	
Transmission (G_{rear})	8.28:1
Peak Power	182 kW (350V)
Peak Motor Torque ($T_{cap-rear}$)	500 Nm

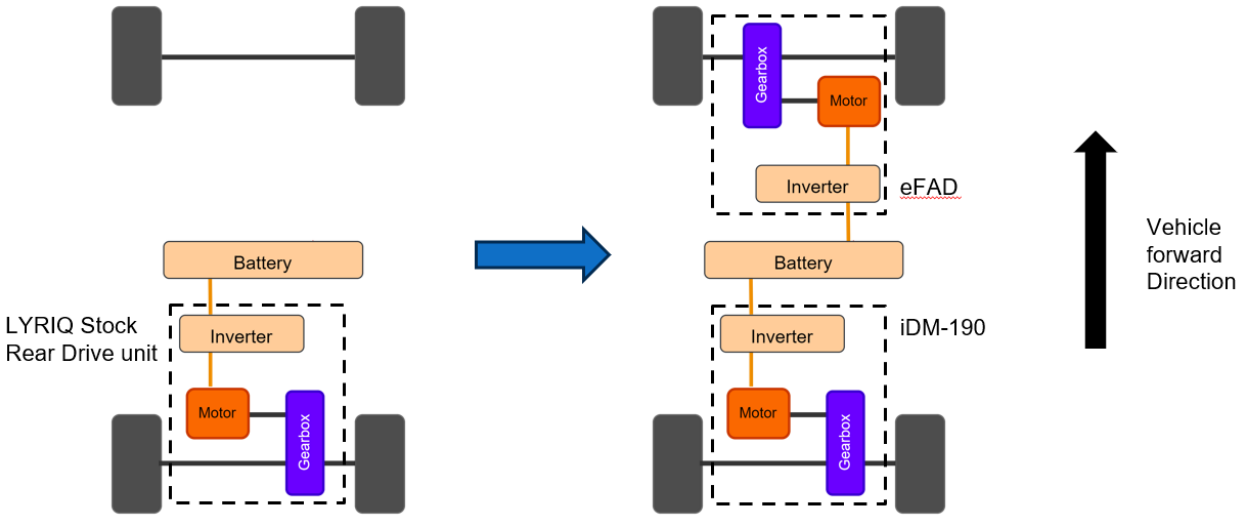

Figure 3.15: Changing the stock 2023 RWD Cadillac LYRIQ architecture to the approved architecture for EcoCAR EV Challenge

Chapter 4

Performance Modeling

Starting with the vehicle development process, modeling was the initial step. The base-vehicle model provided by MathWorks was modified to best represent the architecture being modeled. A simplified schematic of the model is given in Figure 4.1.

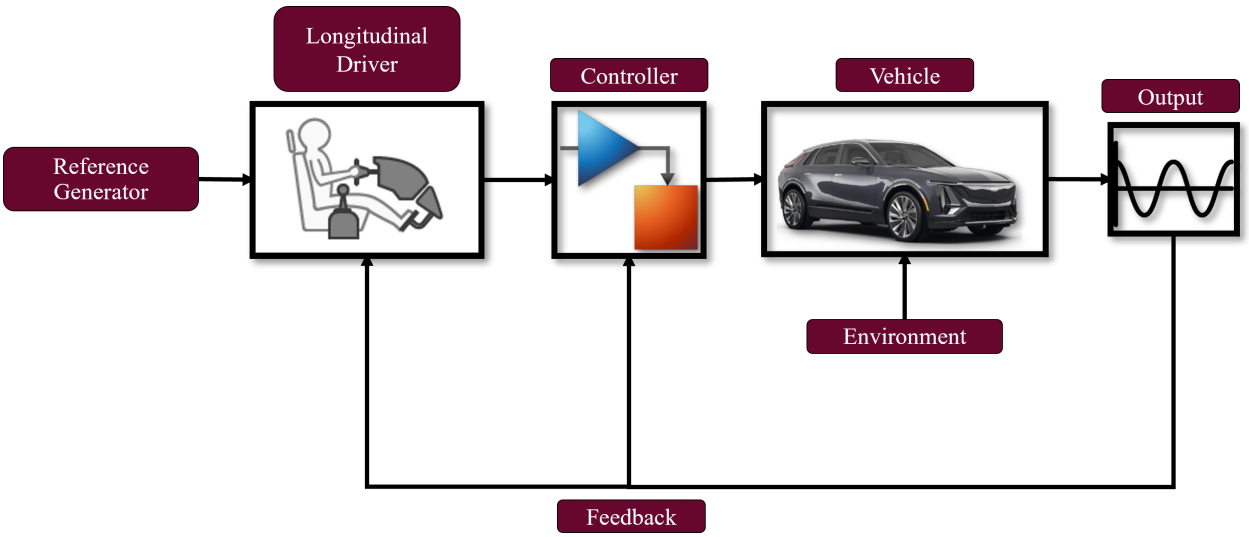

Figure 4.1: Simplified MathWorks model

4.1 Reference Generator

This block generates the reference velocity signal. For example, a drive trace. For this study, custom Wide-open throttle drive traces were used for acceleration and braking performance evaluation. UDDS (Urban Dynamometer Driving Schedule) and HWFET (Highway Fuel-

Economy Test) drive cycles were used for energy consumption evaluations. This is used as the reference input for the model.

4.2 Longitudinal Driver

The driver is a representation of a physical driver, trying to track the reference drive trace. It is important to note that the driver plays a key part in closing the loop. A longitudinal driver block configured for predictive control has been used. It is assumed that the drive mode is set to 'Drive' or 'D', and the propulsion system is enabled throughout the simulation. Vehicle body parameters (which are needed for predictive control) are also set in the driver block. These include vehicle mass, effective rotational inertia, preview time-window, road-load parameters, etc. Ultimately, the driver reads the reference velocity from the reference generator block and actual vehicle velocity from the vehicle body model, to evaluate the error signal and output the accelerator or pedal command to the controller block.

4.3 Controller

The Controller block represents the Propulsion Supervisory Controller. Overall, in the case of the torque architecture, the controller is responsible for reading the pedal-inputs and various sensor signals and translating them to front and rear torque commands for the drive-units. The front and the rear drive-units each have traction inverters. These have local control systems, which regulate current to the motors in the respective drive-units based on the torque commands from the PSC. Please note that the team does not have access to the local control system, but is responsible for transmitting the torque commands to the drive-units. The PSC is also responsible for transmitting functionality information

(such as enable/disable command, intended drive-mode or spin direction, etc.) as well as configuration information. Hence, in the case where the propulsion system is enabled and the electronic transmission range selection has been selected as 'Drive' or 'D', the primary control objective is to read the pedal inputs as well as signals such as like wheel speeds, drive-unit temperatures, HV battery limits, etc. transmitted from other vehicle sensors and controllers and translating these to torque commands for the front and the rear drive-units. In real-time implementation, these torque commands would be transmitted by the PSC to the front and the rear drive-unit inverters. the Limits and derating including HV safety, chassis control and drive unit thermal (along with other functionality features as well as safety features) are also applied by the controller.

4.4 Vehicle Model

The vehicle model block consists of the individual subsystem models including mechanical and electrical sub-systems (vehicle body, wheels, HV battery, suspension, drive-units etc.). It has been built using [34]. The vehicle body is modeled as a glider model.

4.4.1 Vehicle Body Model and wheels

The glider model for the vehicle is shown in Figure 4.2. The 1-degree-of-freedom longitudinal body model has been utilized. The net longitudinal force (F)

$$F = F_{tractive} - F_{grade} - F_{drag} \tag{4.1}$$

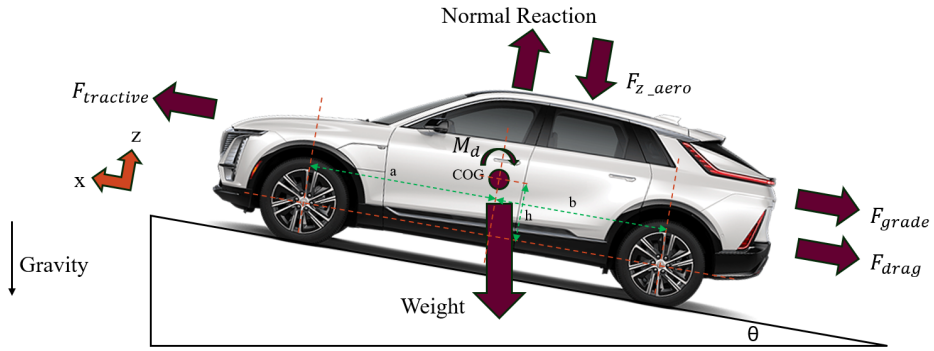

Figure 4.2: Vehicle body glider model

where $F_{tractive}$ is the tractive force, F_{grade} is the gradient force and F_{drag} is the drag force

$$F_{tractive} = F_{x-front} + F_{x-rear} \tag{4.2}$$

where, $F_{x-front}$ and F_{x-rear} are the effective longitudinal forces in the front and the rear axles respectively.

$$F_{grade} = mgsin(\theta) \tag{4.3}$$

where m is the vehicle mass, g is the acceleration due to gravity, and θ is the gradient/slope.

$$F_{drag} = \frac{1}{2}(\rho)(C_d)(A_{front})(v - v_w)^2 \tag{4.4}$$

where ρ is the air density, C_d is the drag-coefficient, A_{front} is the vehicle frontal area, v is the vehicle velocity, and v_w is the longitudinal wind velocity.

The vehicle body block also calculates the vertical force on each axle ($F_{z-front}$ and F_{z-rear}

for the front and rear axles respectively),

$$F_{z-front} = -M_d - h(F_{drag} + mgsin(\theta) + F) + b(mgcos(\theta) + F_{z-aero}) \tag{4.5}$$

and

$$F_{z-rear} = M_d + h(F_{drag} + mgsin(\theta) + F) + a(mgcos(\theta) + F_{z-aero}) \tag{4.6}$$

where, M_d is the torque due to drag (given by $M_d = \frac{1}{2}\rho C_{pm} A_{front}(v - v_w)^2(a + b)$ C_{pm} is the pitch drag moment coefficient, a is the longitudinal distance between the center of gravity and the front axle, b is the longitudinal distance between the center of gravity and the rear axle, h is the center of gravity height above the axles (in the vehicle z-axis).

The wheel model evaluates the effective tractive force by deploying the Magic Formula. The drive unit torque is directly applied to the wheel model. Also, in case of braking, the brake pressure is applied. Rolling resistance is also evaluated in this block. For each wheel, the rolling resistance torque would be

$$M_{rolling} = R_e(A_r + B_r|v| + C_r v^2)(F_z^{\beta})(p_i^{\alpha})(tanh(4v)) \tag{4.7}$$

where F_z is the vertical force at the respective axle, R_e is the effective radius of the wheels, A_r, B_r, and C_r, are the velocity-independent, linear velocity dependent and quadratic velocity dependent force components respectively, and p_i is the tire pressure.

The wheel model also has a disc brake model where, braking torque (T_b) is given by

$$T_b = \frac{\mu P_b \pi B_a^2 R_m N_{pads}}{4} \tag{4.8}$$

where μ is the coefficient of friction between the rotor and the brake pads ($\mu = \mu_{static}$ when rotor RPM = 0, and $\mu = \mu_{kinetic}$), P_b is brake pressure, B_a is brake actuator bore diameter, R_m is mean effective radius N_{pads} is the number of brake pads (= 2, in this case, because there are 2 brake pads per axle).

The interaction between the vehicle body model and wheel model is shown in Figure 4.3.

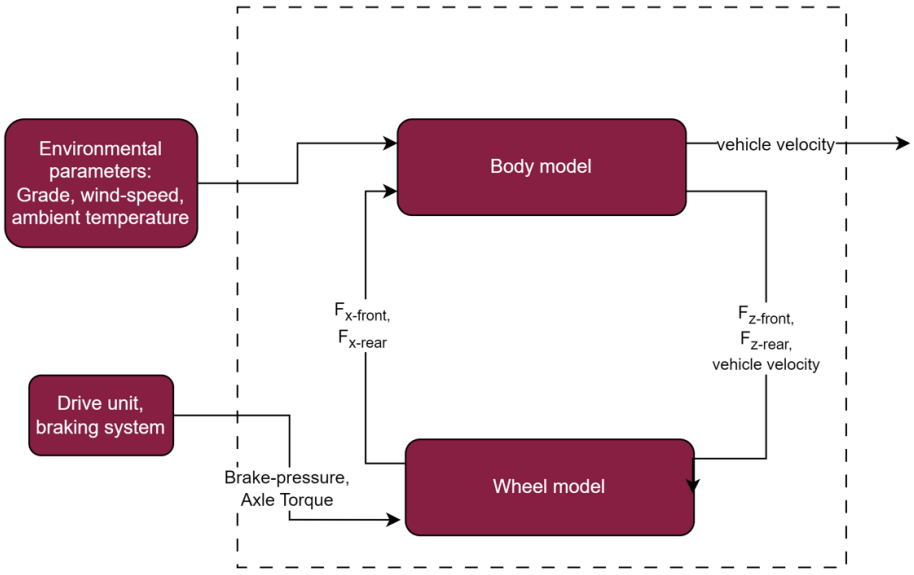

Figure 4.3: Interaction between vehicle and wheel model

4.4.2 Drive unit model

The motors for this study have been modeled using the loss equation in [23]. The motors have mainly been modeled using: copper-loss coefficient (k_c), iron-loss coefficient (k_i), windage-loss coefficient (k_w), and stray-loss (C). Note that these were derived from the drive-unit manufacturer provided and from [28], and set up as motor-inverter combined system loss

models. For the front motor, the power loss is given by:

$$\begin{aligned} P_{loss-front-motor} =& k_{c-front} T_{front}^2 + k_{i-front} \omega_{front} \\ &+ k_{w-front} \omega_{front}^3 + C_{front} \end{aligned} \tag{4.9}$$

Similarly, for the rear motor, the power loss is given by:

$$\begin{aligned} P_{loss-rear-motor} =& k_{c-rear} T_{rear}^2 + k_{i-rear} \omega_{rear} \\ &+ k_{w-rear} \omega_{rear}^3 + C_{rear} \end{aligned} \tag{4.10}$$

where T represents the motor torque (in Nm), and ω represents the motor speed in (rad/s). The drive units are without disconnects and each has a single-speed transmission. The gearbox loss model discussed in [30] has been used for modeling gearbox losses. The front motor gearbox loss is:

$$\begin{aligned} P_{loss-front-gearbox} &= T_{front} \omega_{front} - \\ &(\gamma_{front} T_{front} \omega_{front} - \phi_{front} T_{cap-front} \omega_{front}) \end{aligned} \tag{4.11}$$

where γ represents the gearbox efficiency, and ϕ represents the gearbox loss-coefficient

$$P_{loss-front-gearbox} = ((\gamma_{front} - 1)/\gamma_{front}) T_{front} \omega_{front} + (\phi_{front} T_{cap-front} \omega_{front}) \tag{4.12}$$

The gearbox loss for the rear motor is given by:

$$\begin{aligned} P_{loss-rear-gearbox} &= T_{rear} \omega_{rear} - \\ &(\gamma_{rear} T_{rear} \omega_{rear} - \phi_{rear} T_{cap-rear} \omega_{rear}) \end{aligned} \tag{4.13}$$

For negative axle torques, in case of the rear gearbox the loss is given by

$$P_{loss-rear-gearbox} = ((\gamma_{rear} - 1)/\gamma_{rear})T_{rear}\omega_{rear} + (\phi_{rear}T_{cap-rear}\omega_{rear}) \tag{4.14}$$

4.5 Model Validation

4.5.1 Baseline model results

- Performance modeling The Cadillac LYRIQ 2023, is a production EV, and when the team received the vehicle, it had already been tested. So, simulations for IVM to 60 mph, 50 to 70 mph and the braking distance were completed and compared to test data. Figure 4.4 shows the simulation plots for these vehicle technical specifications.

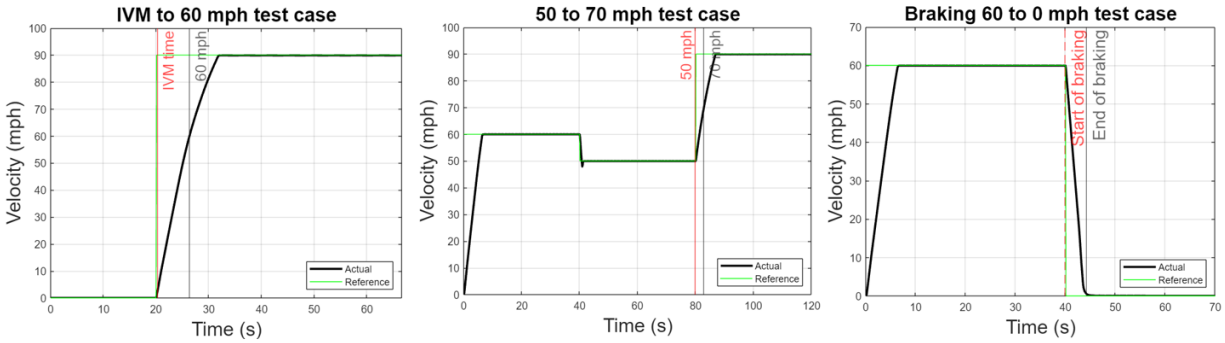

Figure 4.4: Baseline LYRIQ Performance

Table 4.1 shows a comparison of the Vehicle Technical Specifications (VTS) for the stock LYRIQ and those for the model of the stock LYRIQ. Note that the 50 to 70 mph time is slightly off. The reason for that could possibly be a control strategy in the stock LYRIQ, which does not allow the vehicle to accelerate fast at higher speeds. Such a strategy is not applied in the model.

Table 4.1: Comparison of model output with stock LYRIQ Vehicle Technical specifications

Vehicle Technical Specification	Stock LYRIQ	Model Output
IVm to 60 time	5.9 s	6.1 s
50 to 70 mph time	3.9 s	3 s
Braking distance	44 m	50 m

- Energy Consumption Like the performance modeling validation, energy consumption (in terms of unadjusted AC miles per gallons equivalent (MPGe) for city driving (UDDS) and highway driving (HWFET) was used. The EPA reported [2] UDDS MPGe for the stock RWD Cadillac LYRIQ is 136 (UDDS) and 118.1 (HWFET). The model outputs an unadjusted AC MPGe of 122.83 (UDDS) and 109.6 (HWFET). Figures 4.5 and 4.6 show the comparison between the UDDS and HWFET MPGe in the charge depleting mode of the vehicle model and that reported by the EPA, respectively, for the 2023 Cadillac LYRIQ RWD.

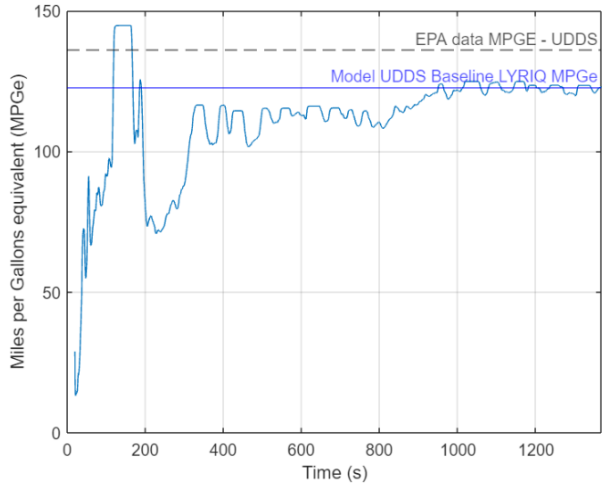

Figure 4.5: Baseline model UDDS MPGe comparison

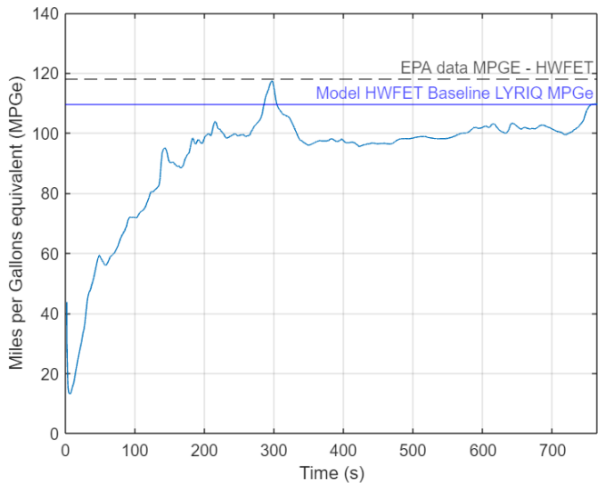

Figure 4.6: Baseline model HWFET MPGe comparison

- Model Correlation with Baseline test data Baseline testing and comparison with the model data is another way to validate the model. For model correlation, [26] states that Normalized Cross-Correlation Power can be used to test a model with respect to logged test data.

$$NCCP = \frac{max(R_{xy})}{max(R_{xx}, R_{yy})} \tag{4.15}$$

Based on equation 4.15, the vehicle was tested, and the vehicle's velocity trace was passed as an input to the model, and parameters like motor torque and current, voltage and State of charge were tested. The drive-cycle speed time trace is shown in Figure 4.7. This was the team developed drive-cycle based on city driving.

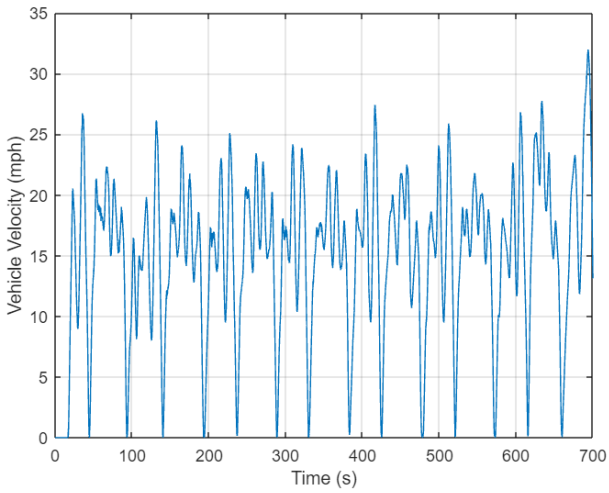

Figure 4.7: Baseline testing - Vehicle velocity trace

The motor torque validation can be seen in Figure 4.8. For motor torque, NCCP = 88.79%

(corrcoeff = 88.63%)

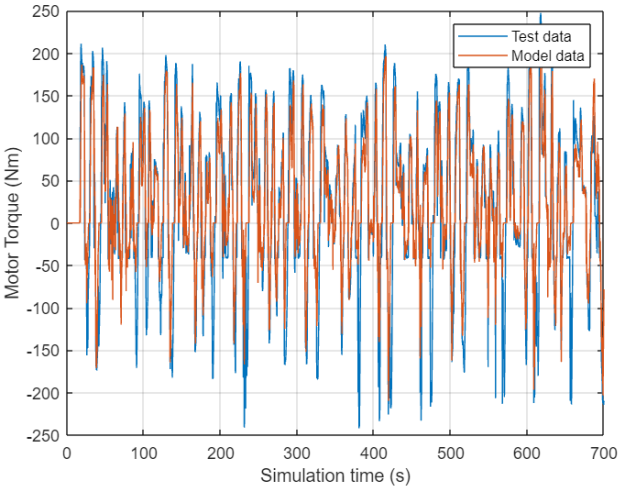

Figure 4.8: Model validation - Motor Torque

The HV Battery current validation can be seen in Figure 4.9. For HV Battery current, NCCP = 93.5%

(corrcoeff = 93.37%)

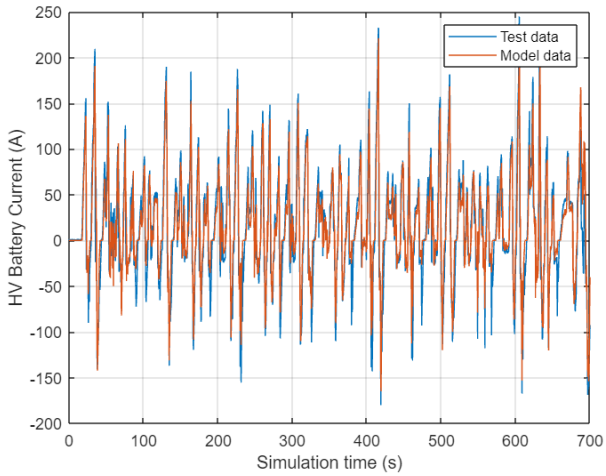

Figure 4.9: Model validation - HV Battery Current

The HV Battery voltage validation can be seen in Figure 4.10. For HV Battery Voltage,

NCCP = 92.13%

(corrcoeff = 92.12%)

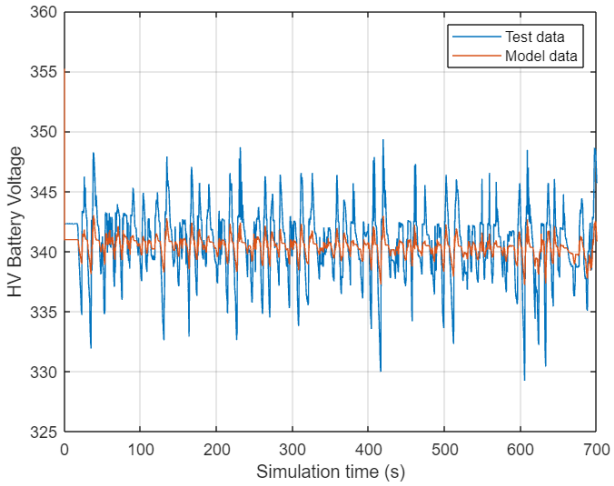

Figure 4.10: Model validation - HV Battery Voltage

The HV Battery SoC validation can be seen in Figure 4.11. For HV Battery SoC,

NCCP = 99.97%

(corrcoeff = 99.97%)

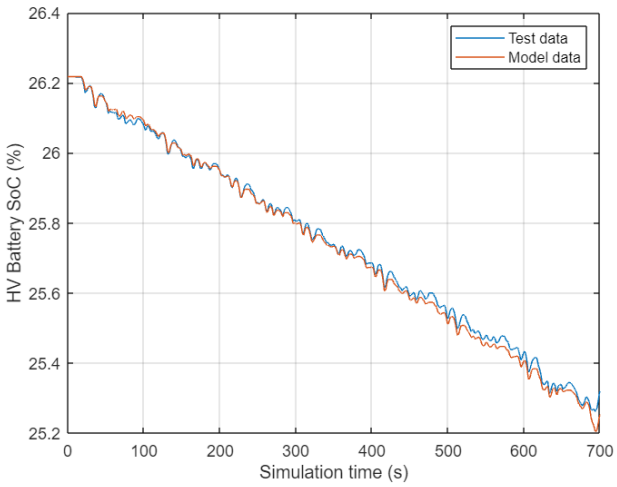

Figure 4.11: Model validation - HV Battery State of Charge

- Sensitivity analysis HEVT would be adding various components, ranging from drive-units, power-distribution system, controllers, etc., which would change the curb mass. Sensitivity analysis was also performed to test how the vehicle's acceleration would respond to a change in mass. The analysis is shown in Figure 4.12.

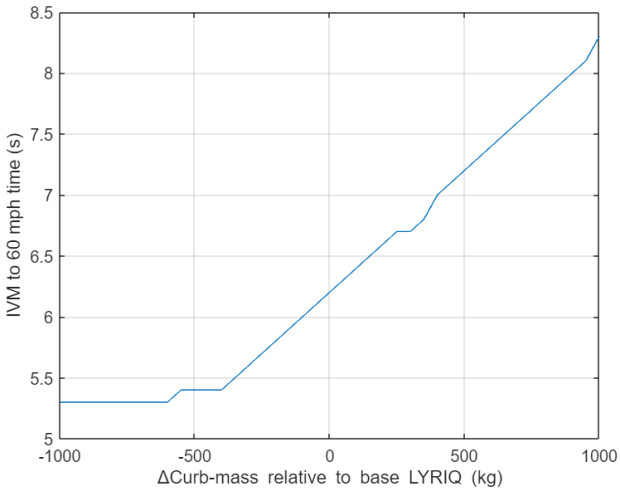

Figure 4.12: Stock LYRIQ - IVM to 60 mph sensitivity analysis

4.5.2 Benchmarking a similar SUV (2021 Ford Mustang Mach-E RWD)

Another method that was used to validate the vehicle was benchmarking a comparable EV - the 2021 Ford Mustang Mach-E RWD Extended range variant. The following were the main changes made to the base model: Battery configuration (i.e., number of cells in series and parallel), battery nominal voltage, battery capacity, vehicle mass and body parameters, and drive-unit model (motor-inverter system parameters and gear ratio).

- Performance modeling The model outputs an IVM to 60 time of 6.6 seconds. Ford has reported a 0 to 60 time of 6.1 seconds [12]. The plot of the IVM to 60 mph acceleration can be seen in Figure 4.13.

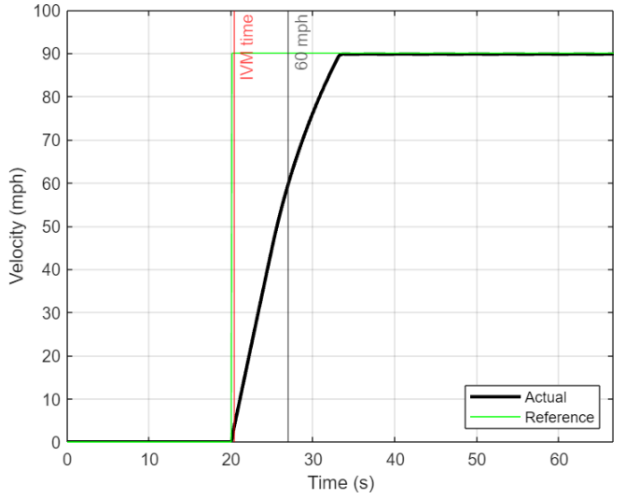

Figure 4.13: 2021 Ford Mustang Mach-E RWD Extended Range - 0 to 60 time

- Energy consumption The EPA reported [1] unadjusted AC MPGe of the 2021 Ford Mustang Mach-E is 146.3 (UDDS) and 127.3 (HWFET). The model modified to represent the 2021 Ford Mustang Mach-E outputs an unadjusted AC MPGE of 130.1 (UDDS) and 113.5 (HWFET). Figures 4.14 and 4.15 show a comparison of the UDDS

and HWFET in the charge depleting mode consumption that the model outputs and that reported by EPA, respectively, for the 2021 Mustang Mach-E.

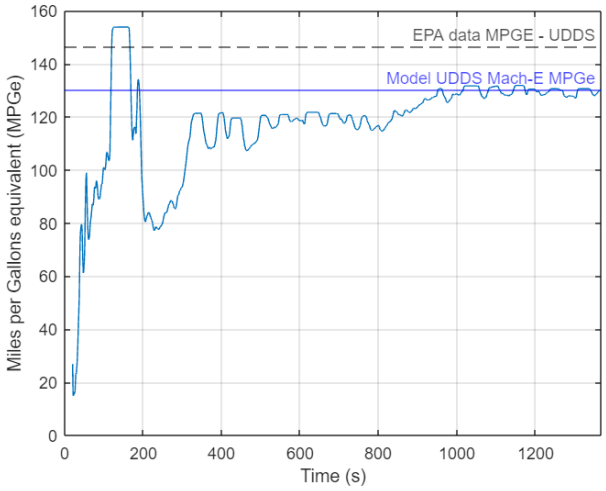

Figure 4.14: Mach-E UDDS MPGe comparison

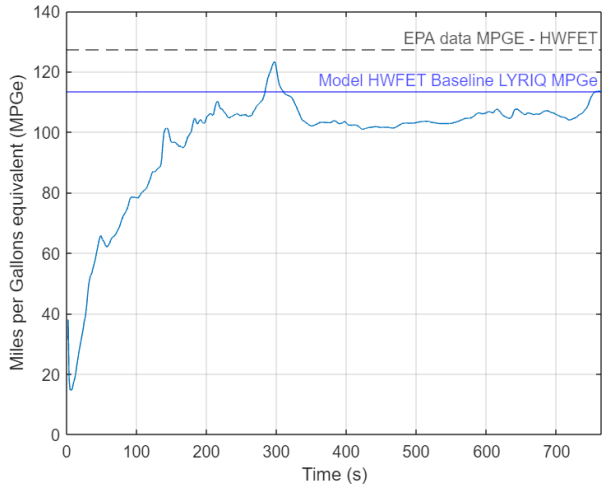

Figure 4.15: Mach-E HWFET MPGe comparison

Chapter 5

Propulsion Controller logic

5.1 Power moding

Power moding refers to the enabling/disabling of the propulsion system. This is one of the most critical features in context of vehicle functionality. For example, the PSC is responsible for requesting the HV Battery contactors to close, the HV bus contactors to close and then to send an inverter enable command, all in the correct order and at the correct times, during a power on sequence. A simplified schematic of the power moding sequence can be seen in Figure 5.1. Please note that Electronic Disconnect Switch (EDS) status and the Isolation Monitoring Device (IMD) i.e. ground fault status are checked i.e., step (2) during the start-up sequence. Also, flags related to the Vehicle Power Mode are checked.

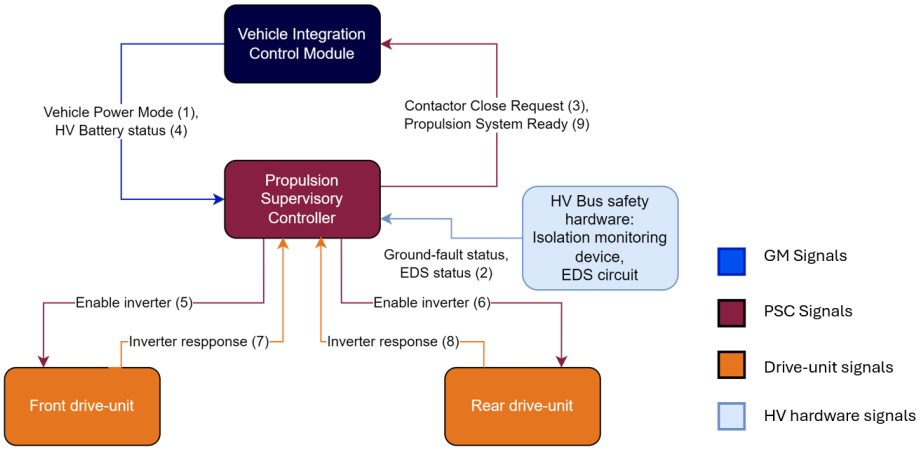

Figure 5.1: Power moding overview

5.2 Electronic Transmission Range Selection

The ETRS logic is responsible for communicating the driver selected range with the drive-units. As an example, a positive or forward torque must be transmitted when the range is set to 'D' or 'Drive' and the accelerator pedal is pressed. For this, when the driver changes the range selection from 'P' or 'Park' to 'D' or 'Drive', the PSC is responsible for ensuring that this range change request is communicated to the drive-units as a direction command. ETRS related flags are checked from the VICM messages. A simplified schematic of the ETRS logic is shown in Figure 5.2.

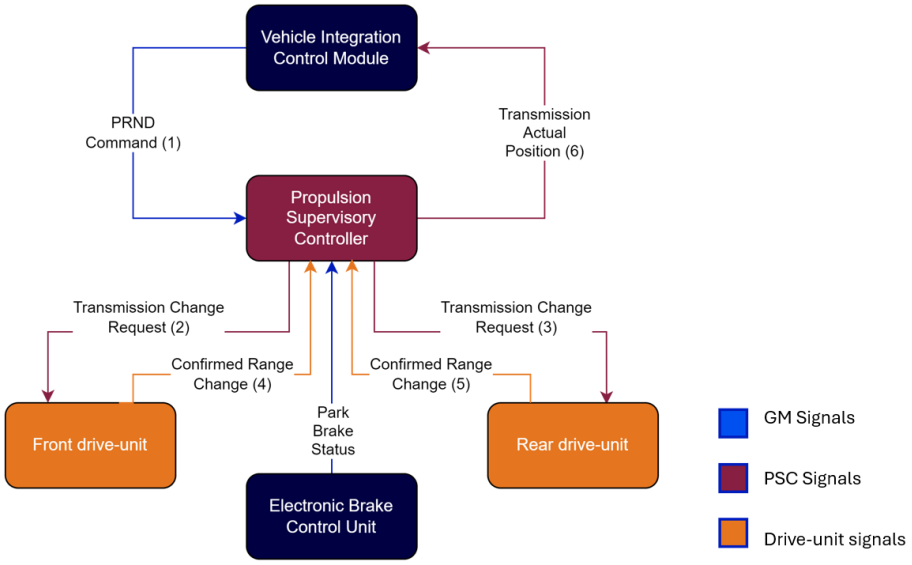

Figure 5.2: ETRS overview

5.3 Torque architecture

Once the vehicle is powered on and the transmission range is selected, the torque architecture logic comes into action. The torque architecture logic is responsible for interpreting the accelerator pedal command along with other sensor signals and transmitting torque com-

mands to both the drive-units. The torque distribution logic is an integral part of the torque architecture. A high-level torque architecture overview can be seen in Figure 5.3.

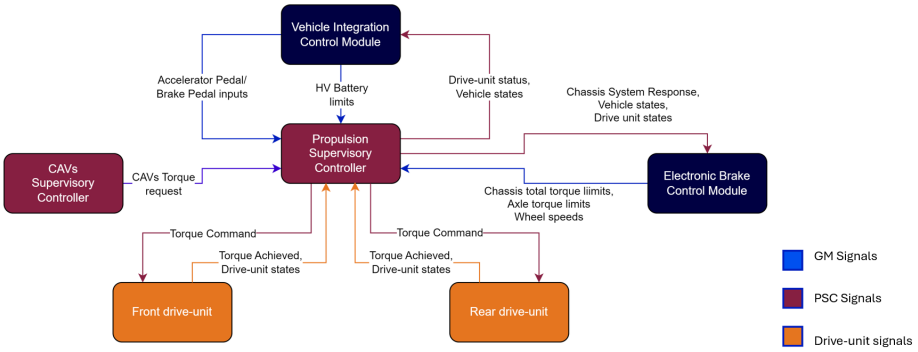

Figure 5.3: Torque architecture overview

A schematic of the torque architecture is shown in Figure 5.4.

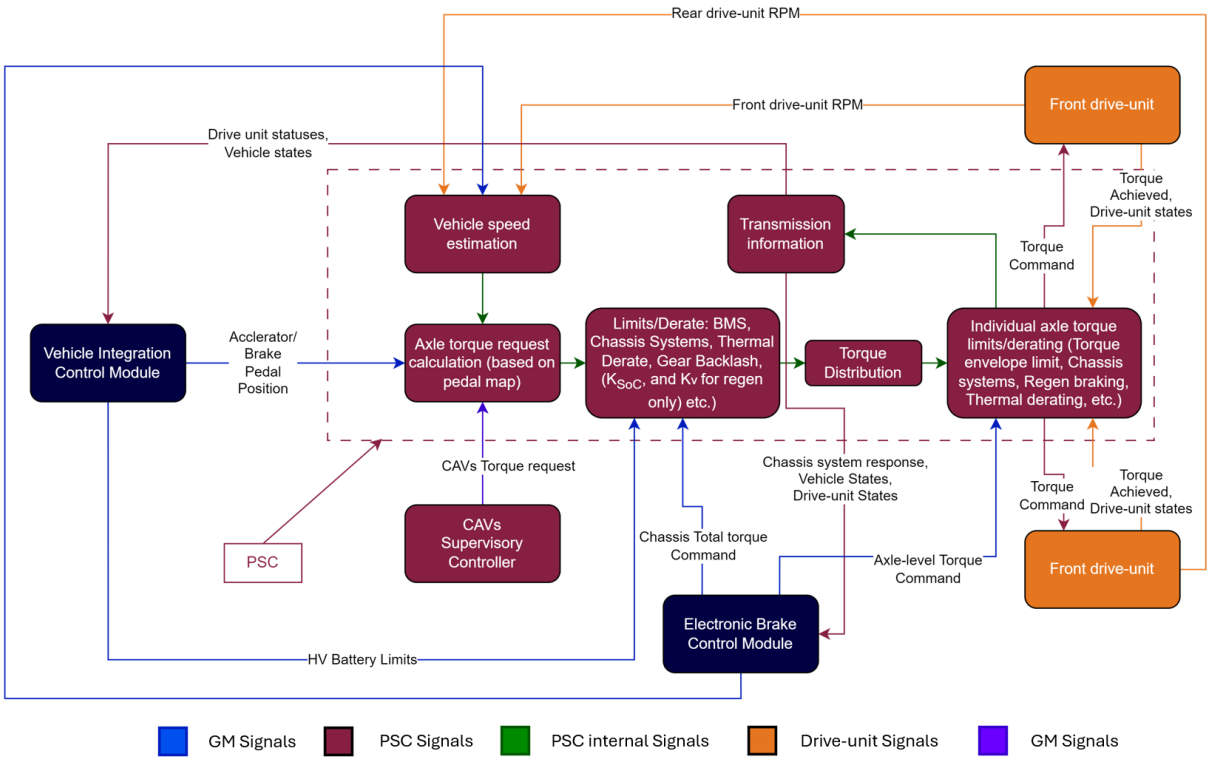

Figure 5.4: Simplified full torque architecture logic

The pedal map (shown in Figure 5.5) is used for evaluating the initial total wheel torque request. The pedal map is based on the ideal torque-speed envelopes of the front (Figure 5.6) and the rear (Figure 5.7) drive-units. The ideal total wheel torque-speed envelope is shown in Figure 5.8. Various limits and derating based on the HV battery (voltage, current and power limits), chassis systems (which includes features like Electronic Stability Control or ESC, traction control and anti-lock braking system), thermal derate strategy etc. are applied on this total intended wheel torque. The torque distribution logic uses this command and converts it to the front and rear drive unit axle torques. Various limits are checked, and some derating factors are applied again (this time in context of the front and the rear axle individually).

The torque speed envelope for the front and the rear drive units are shown below:

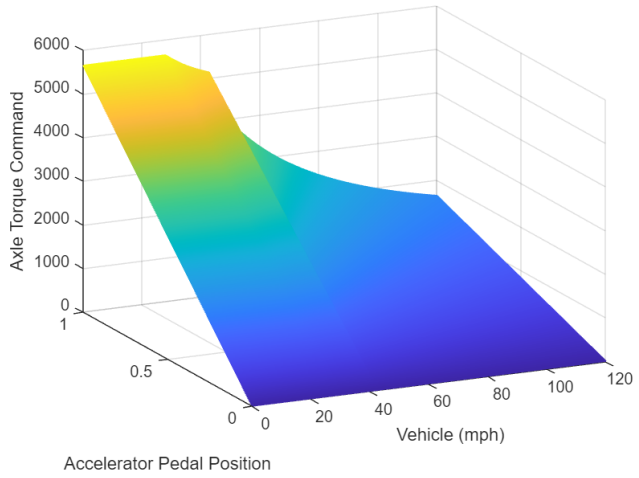

Figure 5.5: Accelerator Pedal-map

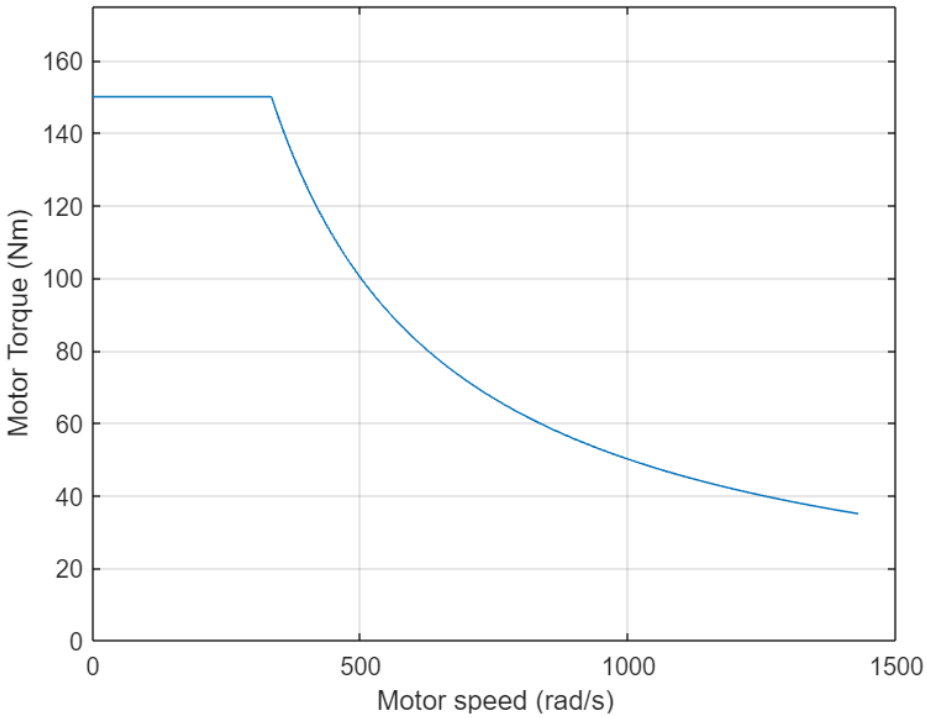

Figure 5.6: Torque speed envelope - front motor

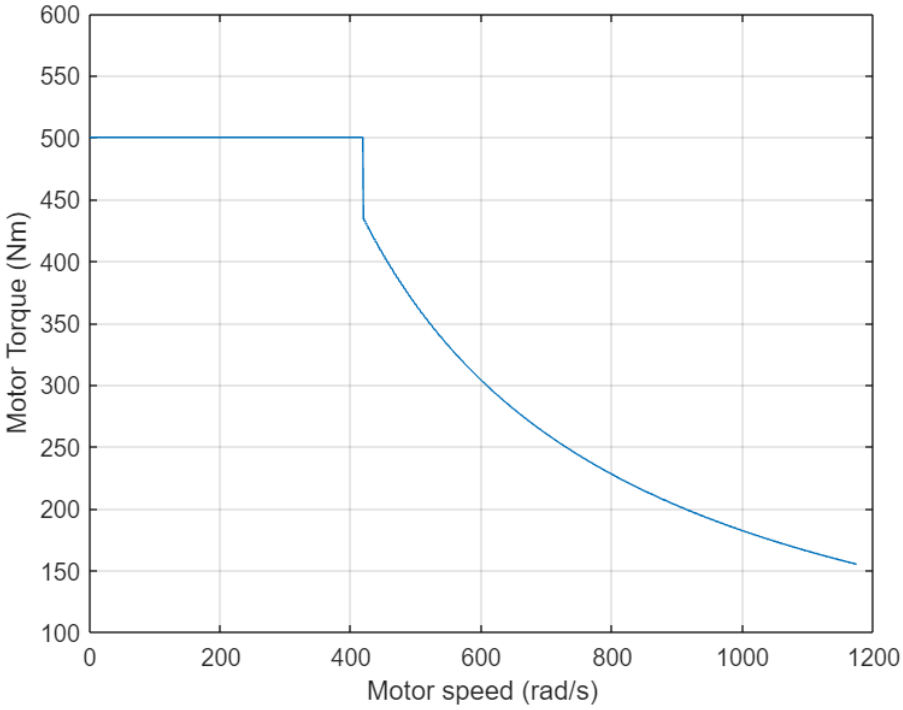

Figure 5.7: Torque speed envelope - rear motor

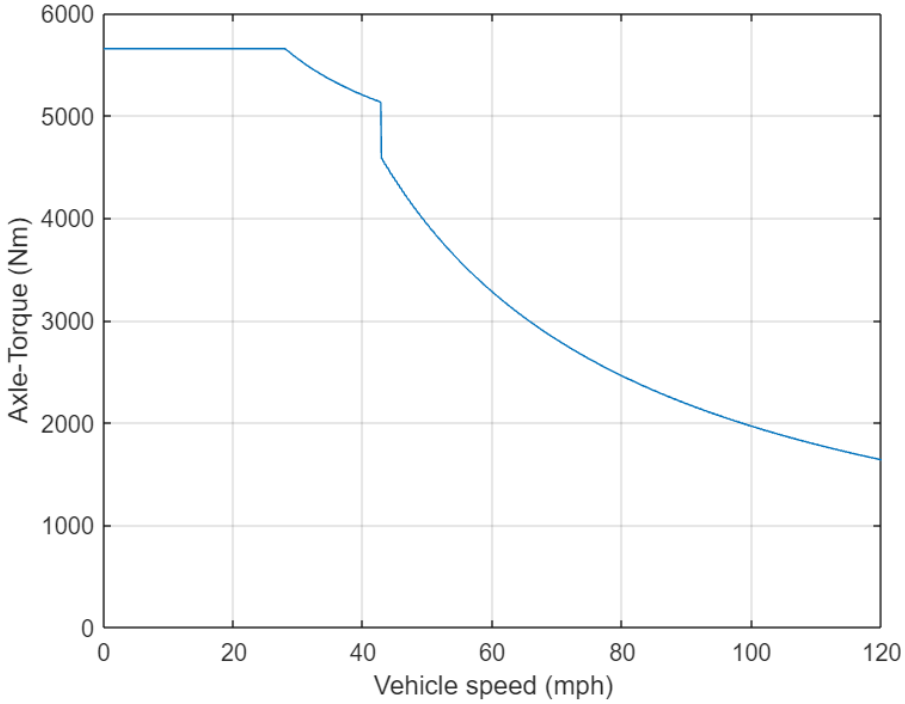

Figure 5.8: Ideal total axle torque speed envelope

As mentioned before, there are 3 main types of limits/derating that need to be applied, in case of the positive torque commands.

1. BMS limits/HV Battery limits: The BMS limits are used to ensure safe operation, with respect to the HV battery.

2. Chassis Systems limit: These correspond to the maximum wheel torque allowed at the wheels to avoid wheel flare and slipping.

3. Thermal derate strategy: It is unsafe to operate the drive-units above certain temperature. Hence, continuously monitoring the drive-unit temperature, to limit, is necessary for ensuring that the drive-units operate safely. A simplified schematic of the thermal derate strategy is shown in Figure 5.9.

The total axle torque is first checked (and derated if needed) and then passed to the torque

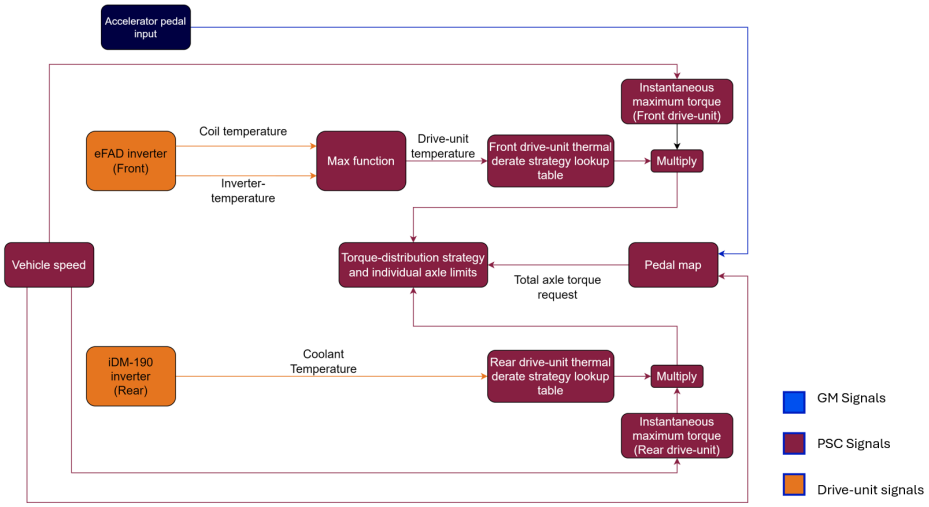

Figure 5.9: Simplified thermal derate strategy logic

distribution strategy. Then, the outcome is checked for individual axle torques limits, considering the drive-unit thermal derating. These limits are calculated by multiplying the initial total wheel torque request with the thermal derate factor. Then the torque commands from the torque distribution strategy are checked for these individual axle torque limits.

Hence, the total axle torque available would be given by

$$\tau_{available} = K_{thermal-front}\tau_{max-front} + K_{thermal-rear}\tau_{max-rear} \tag{5.1}$$

and the individual axle torque limits are $\tau_{front} \leq K_{thermal-front}\tau_{max-front}$ and $\tau_{rear} \leq K_{thermal-rear}\tau_{max-rear}$ where $\tau_{available}$ is the available axle torque, τ_{front} is the front axle torque, τ_{rear} is the rear axle torque, $\tau_{max-front}$ is the maximum instantaneous front axle torque, $\tau_{max-rear}$ is the maximum instantaneous rear axle torque, $K_{thermal-front}$ is the front thermal derate factor, $K_{thermal-rear}$ is the rear thermal derate factor,

The thermal derate factors for the front and the rear drive units are shown in Figures 5.10 and 5.11 respectively.

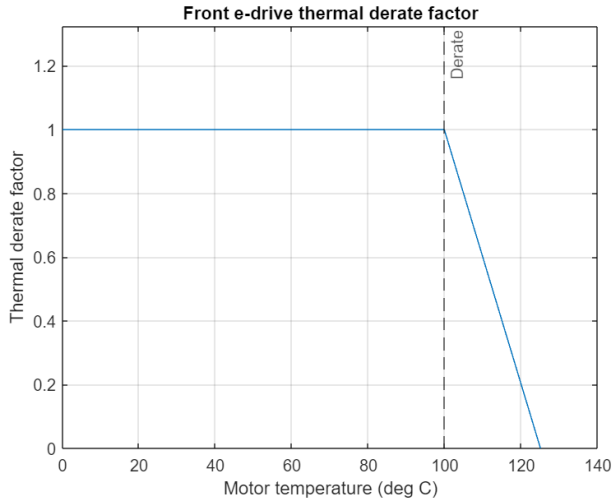

Figure 5.10: Thermal derate strategy for front drive-unit

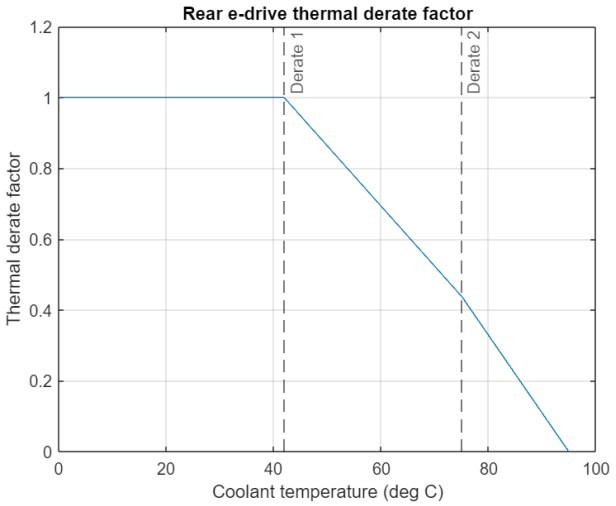

Figure 5.11: Thermal derate strategy for rear drive unit

In the case where one of the axle torque must be derated, the balance torque is requested from the other drive unit (till the limit, with a safety factor). Finally, it is ensured, that both the drive-units are operating within the limits.

In the case of negative axle torques, there are two additional derating factors that need to be implemented for a safe operation. If the vehicle is being operated near full charge, regenerative braking must be disabled, to ensure that the battery does not get overcharged. For this, a derate factor K_{SoC} (Figure 5.12) is introduced. The regenerative braking power is proportional to the motor speed. At low speeds, the drive units are not able to charge the battery. Hence, it is best to derate the available regenerative torque at low speeds, using a speed derate factor K_v (Figure 5.13). This has been discussed in depth in [16]. Hence,

$$\tau_{available} = K_{SoC} K_v \tau_{max} \tag{5.2}$$

where $\tau_{available}$ is the available axle regenerative braking torque τ_{max} is the maximum instantaneous wheel torque (based on the torque-speed envelopes).

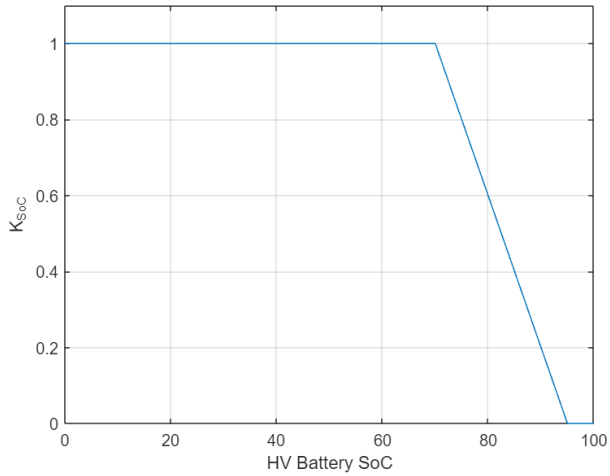

Figure 5.12: Regenerative braking derating - SoC

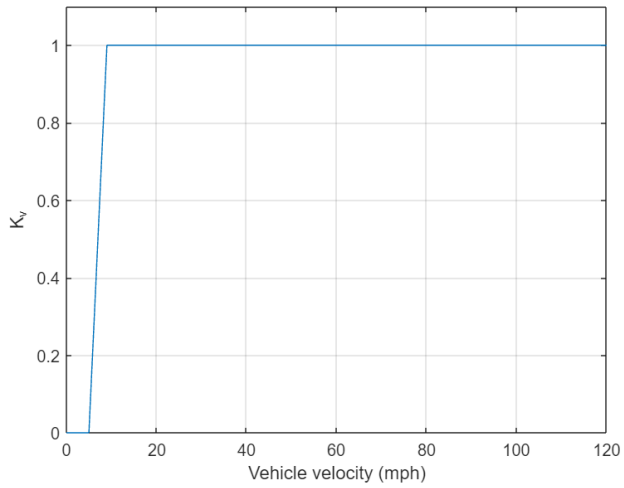

Figure 5.13: Regenerative braking derating - speed

Please note that the speed and SoC derate factors are for the modified LYRIQ and not the base vehicle.

Chapter 6

Torque Distribution Strategy

To finalize the torque distribution strategy, the energy consumption performance of the different strategies was evaluated. Initially, the strategies were evaluated exclusively for propulsion torques, for simplicity. This meant that the drive units only contribute to positive torques, and all the braking torque comes from the mechanical braking system in this case. After that, regenerative braking strategies were also introduced. The energy consumption using the ideal regenerative braking strategy along with the Penalized optimal strategy has also been studied. It is useful to note that the optimal strategies that are discussed result in a mapping, that ultimately utilizes the total wheel torque command (which is calculated from the pedal map, using the accelerator pedal input as well as the instantaneous vehicle speed) and the vehicle speed, to evaluate the torque distribution resulting in the front and rear drive-unit torque commands. The UO and the PO, hence, result in non-linear look-up tables for the torque distribution strategy.

6.1 Unpenalized Optimal Torque Distribution Strategy (UO)

In this strategy, the drive-train losses at all points of operation during the drive-cycle are minimized. This strategy minimizes losses in the motor-inverter gearbox system while meeting

the total axle torque request. The total axle torque request is a function of the instantaneous vehicle speed and pedal input.

$$\begin{aligned}
\min_{T_{front},T_{rear}} \quad & P_{loss-front-motor} + P_{loss-rear-motor} \\
& + P_{loss-front-gearbox} + P_{loss-rear-gearbox} \\
\text{s.t.} \quad & 0 \leq T_{rear} \leq T_{max-rear} \\
& 0 \leq T_{front} \leq T_{max-front} \\
& \tau_{total} = \gamma_{front} T_{front} G_{front} \\
& + \gamma_{rear} T_{rear} G_{rear} \\
& - (\phi_{front} T_{cap-front} G_{front} \\
& + \phi_{rear} T_{cap-rear} G_{rear})
\end{aligned} \tag{6.1}$$

where G represents gear ratio, T_{max} represents instantaneous maximum torque (based on the torque-speed envelope) T_{cap} represents the motor peak torque capacity and τ_{total} represents instantaneous axle-torque (adjusted for gearbox losses).

Initially, when the simulations were carried out exclusively for the positive propulsion torque case. The unpenalized torque distribution strategy for the front and the rear axles is shown in Figures 6.1 and 6.2.

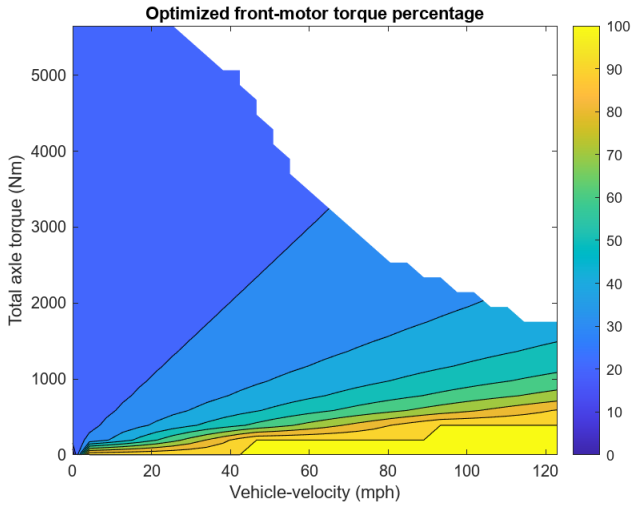

Figure 6.1: Optimal front contribution for positive axle torques

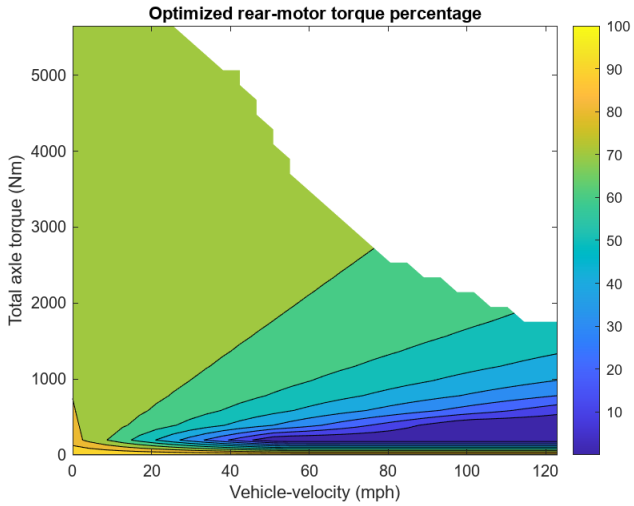

Figure 6.2: Optimal rear contribution for positive axle torques

Including negative axle torques, the unpenalized optimal torque distribution strategy is shown in Figure 6.3 (front) and Figure 6.4 (rear). In the latter case, (where regenerative braking in accounted for), regenerative torque is maximized, and the balance torque is provided by friction brakes.

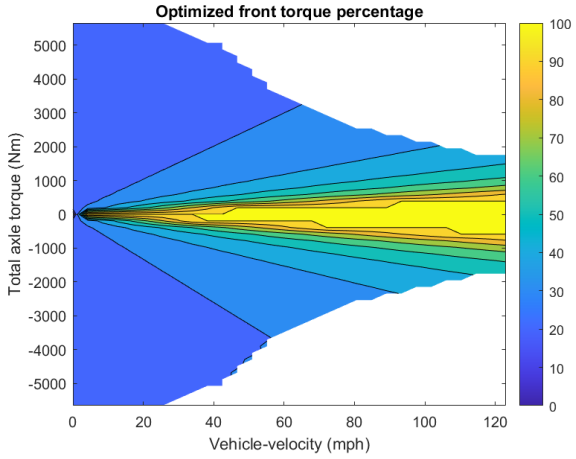

Figure 6.3: Optimized front contribution, including regenerative braking torque

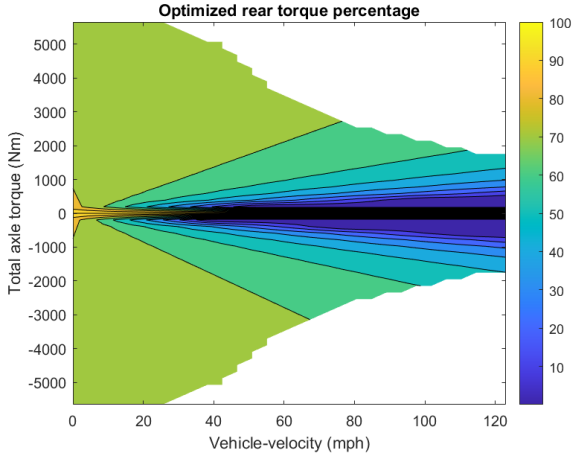

Figure 6.4: Optimized rear contribution, including regenerative braking torque

In the case of UO, the maximum negative torque that can be contributed by the drive-units is used. If the brake torque request corresponds to a torque request greater than the sum of the maximum instantaneous regenerative torque, friction brakes contribute to the balance torque.

6.2 Penalized Optimal Torque Distribution Strategy (PO)

The unpenalized optimal strategy can cause the torque request from any one of the drive units to change values very suddenly, which can cause jerks, ultimately leading to bad drivability.

Hence, a penalty factor is introduced, which adds a cost related to the rate of transfer of power.

This cost can be written as:

$$P_{pwr-rate} = |P(t) - P(t-1)|\lambda \tag{6.2}$$

Hence the strategy can be written as:

$$\begin{aligned}
\min_{T_{front}, T_{rear}} \quad & P_{loss-front-motor} + P_{loss-rear-motor} \\
& + P_{loss-front-gearbox} + P_{loss-rear-gearbox} \\
& + P_{pwr-rate} \\
\text{s.t.} \quad & 0 \leq T_{rear} \leq T_{max-rear} \\
& 0 \leq T_{front} \leq T_{max-front} \\
& \tau_{total} = \gamma_{front} T_{front} G_{front} \\
& + \gamma_{rear} T_{rear} G_{rear} \\
& - (\phi_{front} T_{cap-front} G_{front} \\
& + \phi_{rear} T_{cap-rear} G_{rear})
\end{aligned} \tag{6.3}$$

Here, similar to UO, regenerative torque is maximized, and the balance torque is provided

through friction braking.

6.3 Fixed-Ratio Strategy (FR)

Fixed-ratio torque split refers to a predetermined constant ratio between the front axle and the total axle torque, as well as the rear axle and the total axle torque. To ensure that the maximum torque request can be met, the fixed ratio torque distribution studied here has been set such that the ratio matches that of the case when the maximum torque is requested. Hence,

$$\tau_{rear} = \left(\frac{T_{cap-rear}}{T_{cap-front} + T_{cap-rear}} \right) \tau_{total} \tag{6.4}$$

and,

$$\tau_{front} = \left(\frac{T_{cap-front}}{T_{cap-front} + T_{cap-rear}} \right) \tau_{total} \tag{6.5}$$

From the drive unit manufacturer data, $T_{cap-rear} = 500$ Nm and $T_{cap-front} = 150$ Nm. Hence, for the fixed-ratio torque-split strategy,

$$\tau_{rear} = 0.77\tau_{total} \tag{6.6}$$

$$\tau_{front} = 0.23\tau_{total} \tag{6.7}$$

In this case, since the total torque request is always split into a predetermined ratio, when the individual torque command exceeds the instantaneous maximum axle-torque, the motor which is operating at the limit keeps operating at the limit, and the other motor starts

contributing to the torque request. Once both motors are operating at the limit, the friction braking starts contributing.

6.4 Torque-Assist Strategy (TA)

For the torque-assist strategy, the rear motor is the only motor that provides the torque, until a torque greater than $T_{cap-rear}$ is requested. In case the requested torque exceeds the maximum torque that can be commanded from the rear axle, the balance torque demand is commanded from the front axle. Hence, the strategy can be written as: If $\tau_{total} \leq \gamma_{rear} T_{rear} G_{rear} - \phi_{rear} T_{cap-rear} G_{rear}$,

$$T_{front} = 0 \tag{6.8}$$

Else,

$$\begin{aligned} T_{front} =& (\tau_{total} - \gamma_{rear} G_{rear} T_{max-rear} \\ &+ (\phi_{front} G_{front} T_{cap-front} \\ &+ \phi_{rear} G_{rear} T_{cap-rear}))/(\gamma_{front} G_{front}) \end{aligned} \tag{6.9}$$

where T_{max} represents the instantaneous maximum torque, based on the torque-speed envelope and τ_{total} represents the total axle torque required.

In the later case where regenerative braking is also included.In that case, during regenerative braking, the front motor provides all the regenerative torque, until it is operating at its limit, at which point, the rear drive unit starts contributing to the regenerative torque. This is to mitigate the effects of rear-axle lockup.

The strategy is as follows If $\tau_{total} \leq \frac{T_{front}G_{front}}{\gamma_{front}} - \phi_{rear}T_{cap-rear}G_{front}$,

$$T_{rear} = 0 \tag{6.10}$$

Else,

$$\begin{aligned} T_{rear} =& \frac{\gamma_{rear}}{G_{rear}}(\tau_{total} - \frac{T_{front}G_{front}}{\gamma_{front}} + (\phi_{front}G_{front}T_{cap-front} \\ &+ \phi_{rear}G_{rear}T_{cap-rear})) \end{aligned} \tag{6.11}$$

In the negative torque domain for TA, in case the total torque request exceeds the sum of the instantaneous maximum axle torques for the front and the rear drive-units, the friction brakes start contributing to the total braking torque.

6.5 Penalized Optimal Positive Torque combined with Ideal Regenerative Braking strategy (POIR)

In this case, the penalized optimal torque distribution strategy was utilized for positive axle torque requests. In case of the PO for negative axle torque requests, vehicle stability is not considered. For incorporating stability, the ideal braking curve for the vehicle was evaluated. The ideal braking curve is discussed in [14]. In case of negative axle torque requests, an ideal braking force strategy was utilized.

$$F_{bf} = \frac{a - \frac{2h_g}{mg}F_{br} - \sqrt{a^2 - \frac{4Lh_g}{mg}F_{br}}}{\frac{2h_g}{mg}} \tag{6.12}$$

where m is the vehicle mass, F_{bf} is the front axle braking force, F_{br} is the rear axle braking force, a is the longitudinal distance between the center of gravity and the front axle, h_g is the height of the vehicle's center of gravity above the ground, L is the wheelbase.
Based on this, the ideal braking torque-distribution curve for the modified vehicle is shown in Figure 6.5.

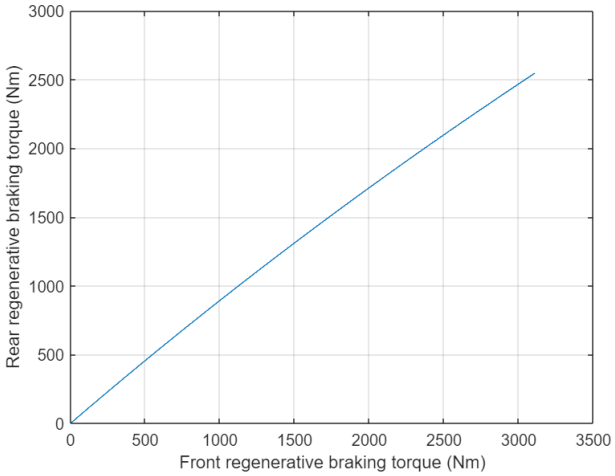

Figure 6.5: Ideal regenerative braking curve

In this case, the total regenerative braking torque is limited by the front motor. Hence, the rear motor never contributes to regenerative braking torque at full capacity. At a braking torque request that exceeds the sum of the maximum instantaneous front axle regenerative torque and the corresponding instantaneous rear axle braking torque, the friction brakes contribute with the balance torque to meet the total torque request.

6.6 Penalized Optimal Positive Torque combined with Torque-Assist Regenerative Braking strategy (POTA)

In this case, the penalized optimal torque distribution strategy would be used for positive torque requests and the torque assist regenerative braking strategy would be used when braking. The torque assist strategy during regenerative braking would mean that only the front drive-unit would contribute to the regenerative braking, till it is operating at its maximum capacity, after which the rear-motor would start contributing with the regenerative braking. [14] states that it is better from a stability standpoint to remain under the ideal braking distribution curve, and in this case, because most of the regenerative torque is being provided by the front drive, the operation points are always below the ideal regenerative curve.

Chapter 7

Simulation

Table 7.1 shows the simulation parameters being applied to all the simulations for this study. An initial HV battery state of charge of 50% ensures that the HV battery voltage stays close to the nominal voltage of 350V. The environmental parameters like the grade, wind velocity, ambient temperature and air pressure were kept as constants for all simulations, to ensure consistency.

Table 7.1: Simulation parameters

Initial Battery SoC	50%
Vehicle mass	2750 kg
Battery capacity	102 kWh
Nominal Battery voltage	350 V
Wind velocity	0 m/s
Grade	0 degrees
Ambient Temperature	298K
Air Pressure	101325 Pa

Initially, a UDDS drive cycle was used to evaluate the performance of the four torque distribution strategies for testing the case of positive axle torques only. The velocity traces for UDDS using the TA, FR, UO and PO can be seen in Figure 7.1. This validates that the vehicle is able to keep up with the drive cycle under study. Similarly, drive-trace validation has been performed when testing all other cases.

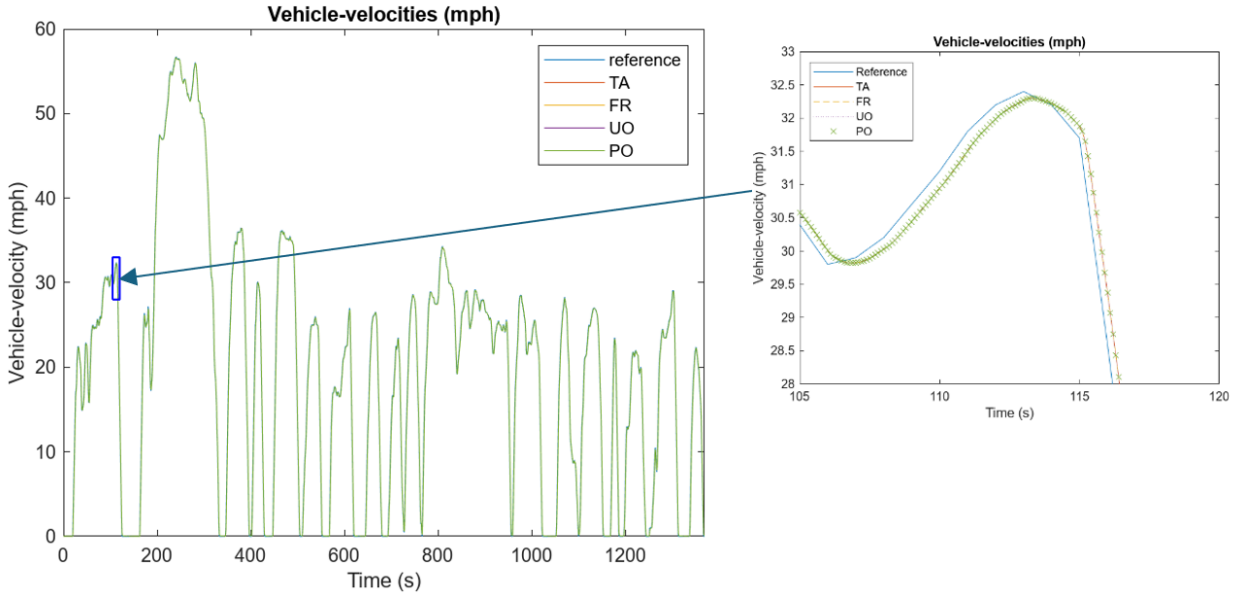

Figure 7.1: Drive-trace validation for positive axle torques - UDDS

The UDDS torque traces for the TA, FR, UO and PO, exclusively for positive torque, can be seen in Figure 7.2. Since regenerative braking was initially disabled, it can be observed that negative torque commands are not being sent to the motor.

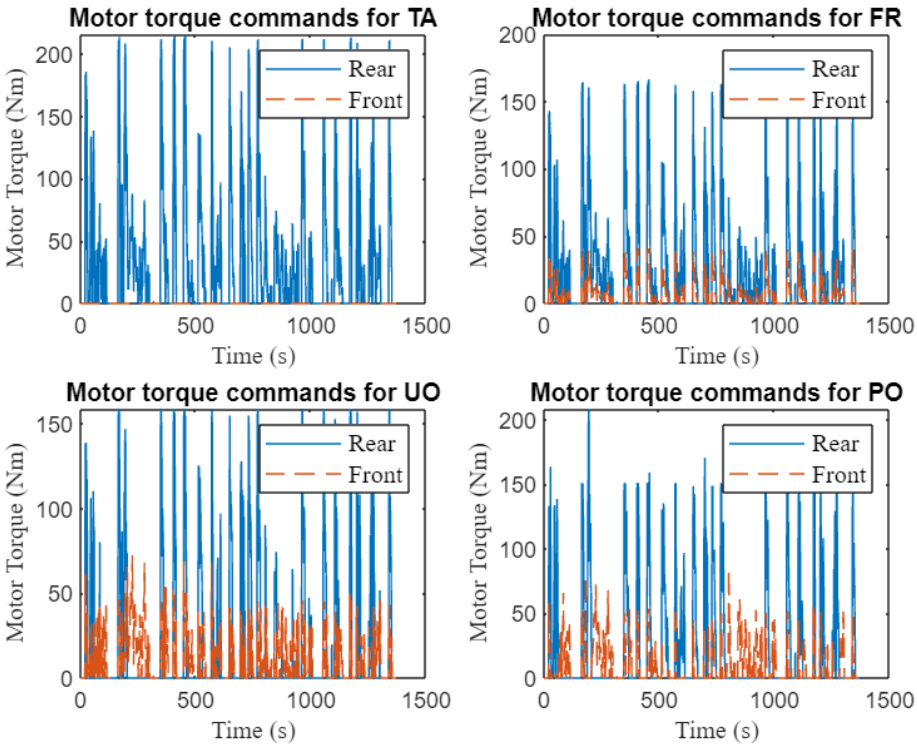

Figure 7.2: Torque traces for Positive Torques - UDDS

Then FR, TA, UO and PO including regenerative braking are tested. The UDDS torque traces for the TA, FR, UO and PO are shown in Figure 7.3. It can be seen that negative toque commands are also being sent by the PSC to the drive units, because the regenerative braking has been in this case.

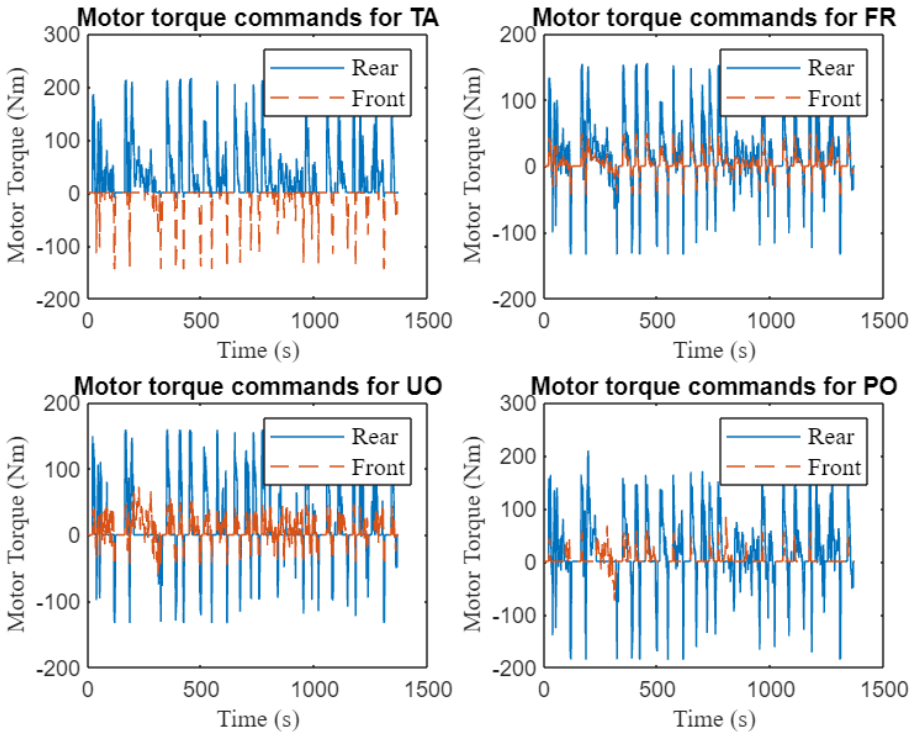

Figure 7.3: Torque traces for UDDS including regenerative torques

Finally, the performance using the penalized optimal strategy (for positive torques), combined with the regenerative braking torque assist strategy, and the ideal braking regenerative torque strategy is compared.

The torque assist regenerative braking strategy utilizes the front motor for regenerative braking, till it is already operating at its limit, after which the rear motor assists the front motor in braking. The penalized optimal strategy (for positive torques) when combined with this is referred to as POTA.

In the ideal braking regenerative braking strategy, the ideal braking distribution curve is followed, and the torque is distributed accordingly. The penalized optimal strategy (for positive torques) when combined with this is referred to as POIR.

It is important to note that these strategies are being compared, because both of them are relatively better from a lateral stability standpoint. Figure 7.4 shows the UDDS torque

traces for the POIR and POTA.

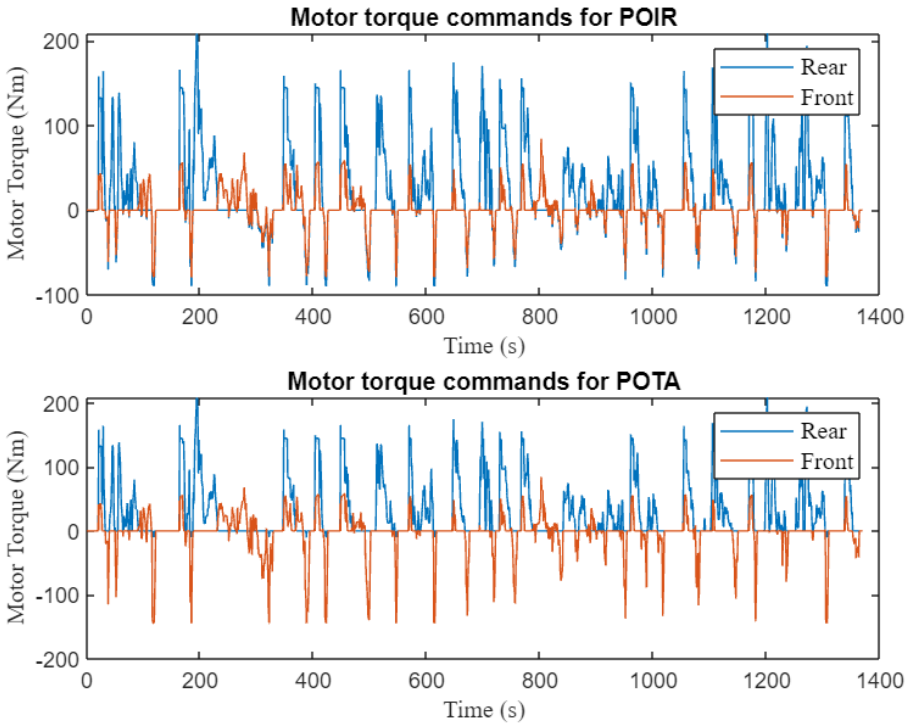

Figure 7.4: Torque traces for POIR and POTA - UDDS

Chapter 8

Results

8.1 Performance - Positive torque (UDDS)

Initially, the different torque distribution strategies exclusively considering positive torques (namely TA, FR, UO and PO) have been compared over UDDS (note that this has previously been published in [20]). The UDDS energy consumption (in kWh/100 miles) with the regenerative braking disabled is shown in Figure 8.1. The simulated energy consumption is highest when using the fixed ratio strategy, which is relatively simpler from a computation standpoint. This is followed by the torque-assist strategy. The unpenalized optimal strategy results in the least energy consumption, since it allows for the drive-units to operate comparatively closer to the most efficient operating points of the drive-units.

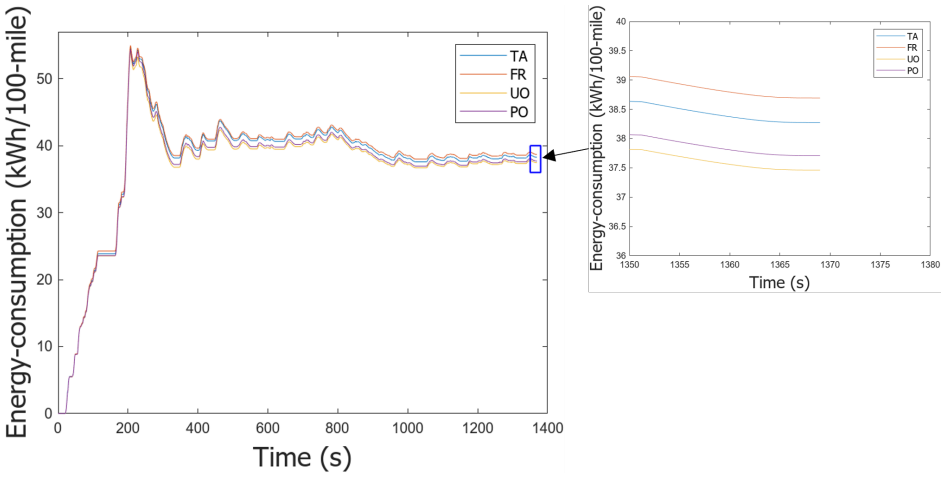

Figure 8.1: UDDS Energy Consumption - Positive Torques

A summary of the energy consumption results for the UDDS, exclusively for positive torques or forward torques, is given in Table 8.1. It can be observed that the PO reduces the energy consumption by 1 kWh/100-miles as compared to a relatively simpler strategy like the FR.

Table 8.1: Summary of Energy Consumption results (UDDS) - Positive Torques

Torque-distribution strategy	Energy Consumption
TA	38.3
FR	38.7
UO	37.5
PO	37.7

The vehicle's state of charge directly depends on the energy consumption. It is important to note that the Cadillac LYRIQ is an all-electric vehicle, and only operates in a charge depleting mode. As the vehicle traverses the distance in the drive-cycle, it consumes energy directly from the HV Battery, and this results in a state-of charge depletion. Figure 8.2. shows the State of Charge plot with respect to simulation time for the UDDS (exclusively considering positive torques). Since regenerative braking has been disabled, no power is sent back to the HV battery while braking.

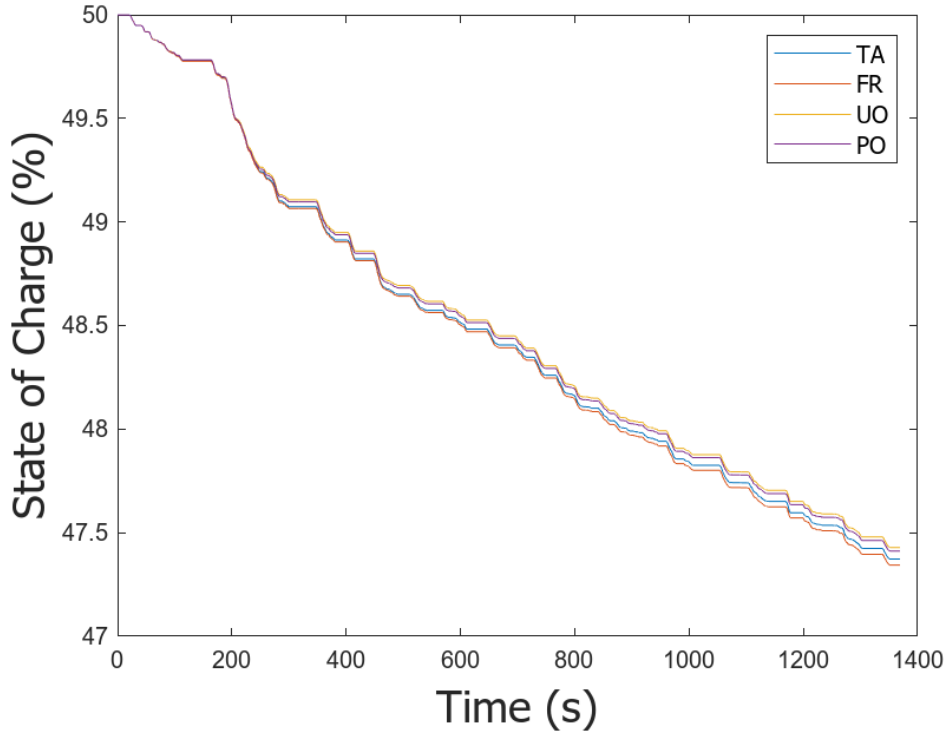

Figure 8.2: UDDS HV Battery SoC Time trace - Positive torques

8.2 Performance - Including regenerative braking Torque (UDDS)

The UDDS energy consumption (in kWh/100 miles) including regenerative braking is shown in Figure 8.3. A similar trend as compared to the case where the regenerative braking was disabled is observed. The fixed ratio strategy has the highest energy consumption, followed by the torque-assist strategy, followed by the penalized optimal strategy. It can be observed that the unpenalized optimal strategy, again, has the least energy consumption.

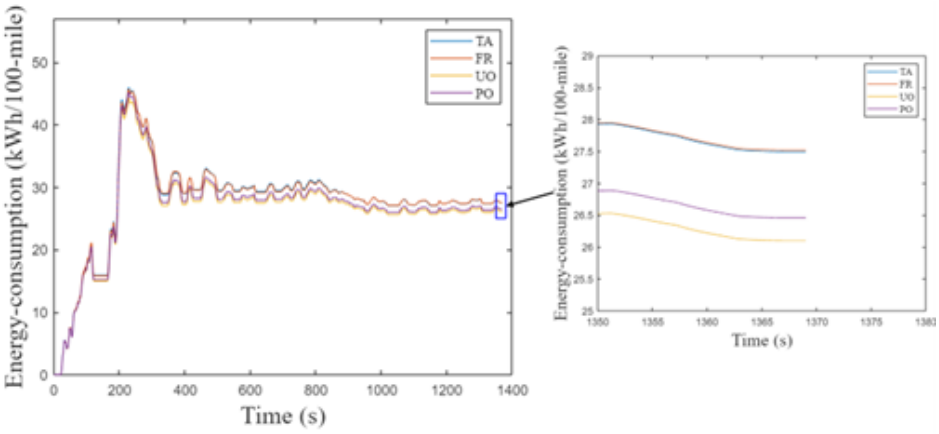

Figure 8.3: UDDS Energy Consumption - Including regenerative braking Torque

A summary of the energy consumption results for UDDS including regenerative braking is provided in Table 8.2.

Table 8.2: Summary of Energy Consumption results (UDDS) - including regenerative braking

Torque-distribution strategy	Energy Consumption (kWh/100-miles)
TA	27.49
FR	27.51
UO	26.1
PO	26.45

In this case, where the regenerative braking is also being considered, power is sent back to the HV battery. The motor functions as a generator when braking, and converts mechanical power (rotational) to AC electrical power. The inverter converts this AC power to DC and transfers it to the HV battery (through a converter). The State of charge of the HV battery hence rises when the vehicle is braking. A plot of the State of Charge of the HV battery with respect to simulation time, for the UDDS including regenerative braking, is shown in Figure 8.4.

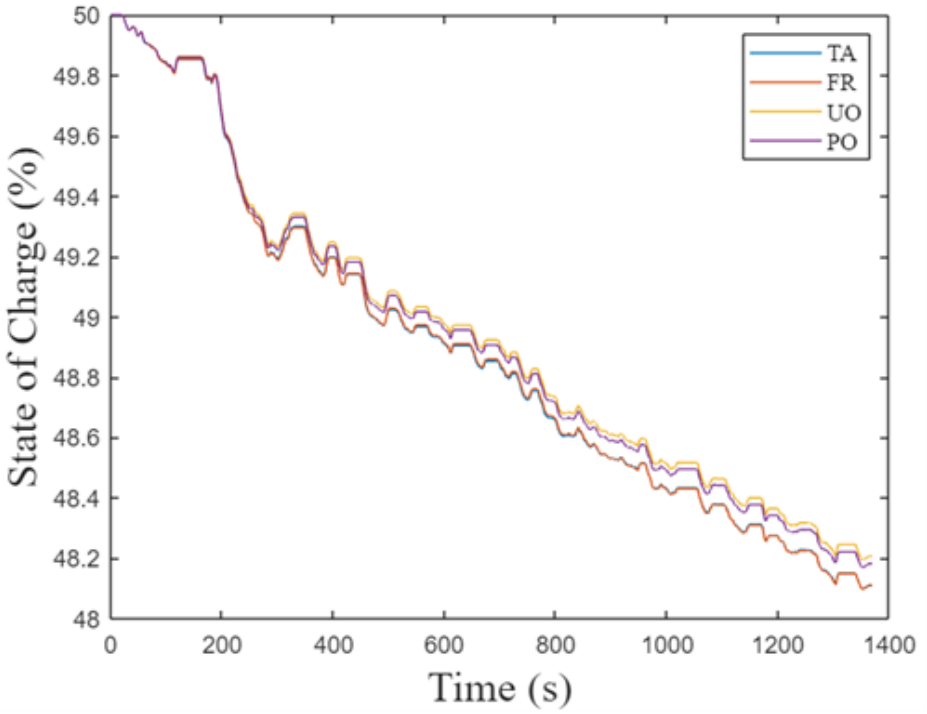

Figure 8.4: UDDS HV Battery SoC Time trace - Including regenerative braking torques

8.3 A comprehensive comparison between PO, and FR with and without regenerative braking for UDDS and HWFET

Comparing PO and FR for UDDS and HWFET would give an overview of how these strategies perform overall and would be key in evaluating the effectiveness of using an optimal strategy over a simple fixed-ratio strategy. Also, the comparison of the cases with and without regenerative braking gives a context about how the regenerative braking improves the vehicle's range. A comparison of the energy consumption for FR and PO over UDDS, with and without regenerative braking, can be seen in Figure 8.5.

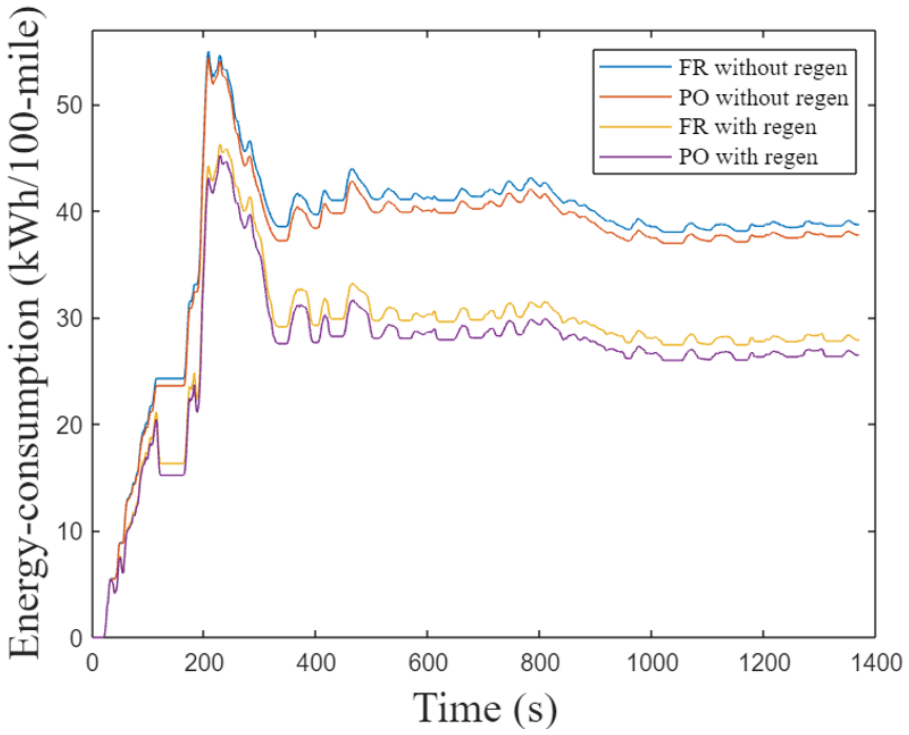

Figure 8.5: UDDS energy consumption comparison between FR and PO with and without regenerative braking

A summary of the energy consumption results for the comparison, over UDDS is provided in Table 8.3.

Table 8.3: Summary of comparison between PO and FR with and without regenerative braking (UDDS)

Torque-distribution strategy	Energy Consumption (kWh/100 miles)
FR positive torque	38.7
PO positive torque	37.7
FR including regenerative braking	27.5
PO including regenerative braking	26.5

Similarly, a comparison of the energy consumption using FR and PO with and without regenerative braking over HWFET can be seen in Figure 8.6.

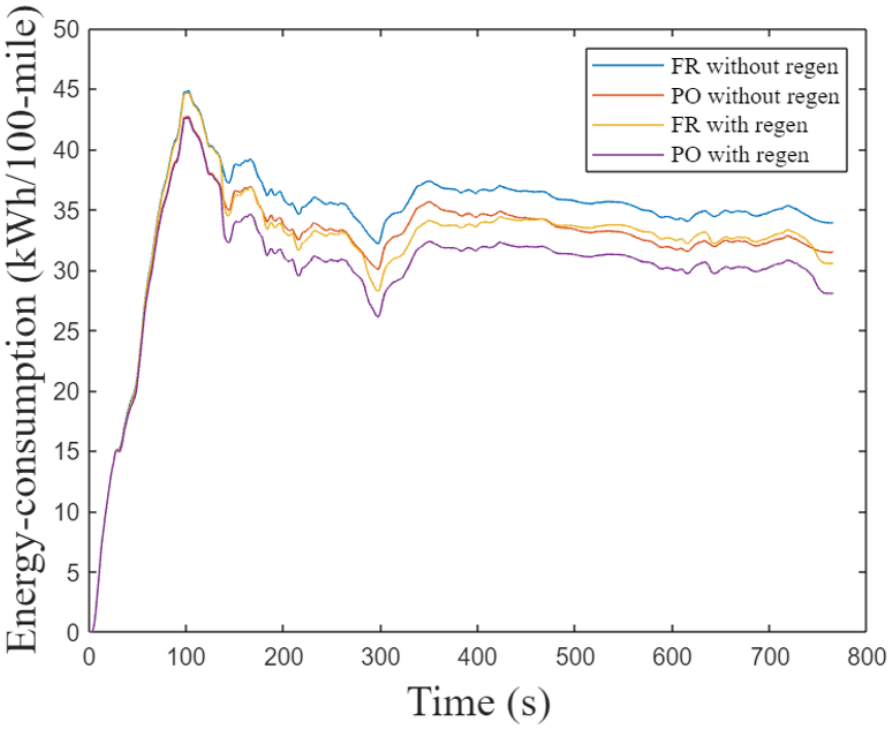

Figure 8.6: HWFET energy consumption comparison between FR and PO with and without regenerative braking

A summary of the energy consumption results for the comparison, over HWFET is provided in Table 8.4.

Table 8.4: Summary of comparison between PO and FR with and without regenerative braking (HWFET)

Torque-distribution strategy	Energy Consumption (kWh/100 miles)
FR positive torque	33.9
PO positive torque	31.4
FR including regenerative braking	30.5
PO including regenerative braking	28.0

Overall, regenerative braking (considering the average for FR and PO) improves the combined adjusted range by around 27%.

The combined range is calculated as a weighted average of the UDDS range and the HWFET

range.

$$range_{combined} = w_{UDDS} range_{UDDS} + w_{HWFET} range_{HWFET} \tag{8.1}$$

where $range_{combined}$ is the combined range, $range_{UDDS}$ is the UDDS range, $range_{HWFET}$ is the HWFET range, $w_{UDDS} = 0.55$, and $w_{HWFET} = 0.45$,

For calculating the individual drive-cycle range,

$$range = 100 \left(\frac{Capacity_{Battery}}{EC} \right) \tag{8.2}$$

where, $range$ is the range for the particular drive-cycle (in miles), $Capactiy_{Battery}$ is the battery capacity (in kWh) and EC is the energy-consumption (in kWh/100-miles).

Also, adjusting for real-world driving,

$$range_{combined-adjusted} = 0.7(range_{combined-simulated}) \tag{8.3}$$

8.4 Performance evaluation of POIR and POTA

From preliminary evaluations, the penalized optimal (PO) strategy, for positive torque commands is chosen for deployment on the PSC. For the regenerative braking torques, it is important to consider lateral stability. According to [37], a front axle lockup does not cause directional instability, because of a self-correcting moment about the vehicle's center of gravity. This does not happen in case of a rear axle-lockup. Hence, it must be ensured that the rear-axle regenerative braking force does not exceed the front axle regenerative force, caus-

ing the rear axle to potentially lockup first. Hence, the torque assist regenerative braking strategy also makes sense, because the front drive-unit is used to the maximum capacity in that case.

Also, according to [14], adhering to the ideal braking curve results in both axles to lockup at the same time, which gives the best driving experience. The proposed ideal regenerative braking strategy adheres to the ideal braking curve.

A combination of PO (for positive torques) with the torque assist regenerative braking strategy is referred to as POTA. A combination of PO (for positive torques) with the ideal regenerative braking strategy is referred to as POIR. POTA and POIR are explored in this section. Figures 8.7 and 8.8 show the UDDS and HWFET energy consumption performance, respectively, using the POIR and POTA.

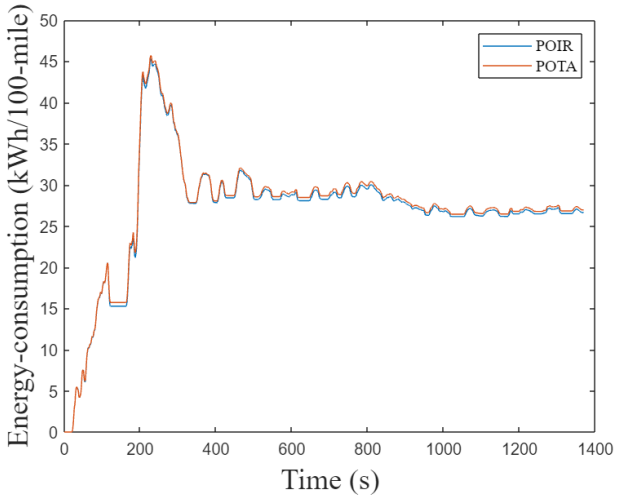

Figure 8.7: UDDS Energy Consumption (kWh/100-miles for POIR and POTA)

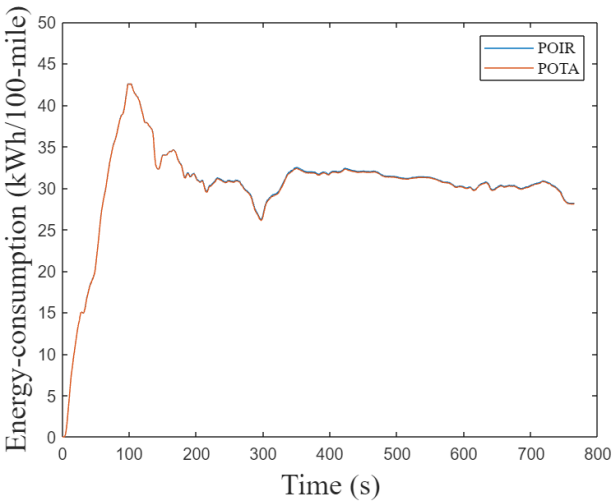

Figure 8.8: HWFET Energy Consumption (kWh/100-miles for POIR and POTA)

A summary of simulated combined adjusted range using all strategies that were considered by HEVT (namely FR, PO, POIR and POTA), for deployment in the torque architecture logic within the PSC, are shown in Table 8.5. Please note that the energy consumption values used for calculating the combined adjusted range were used directly from the simulation log, and had a greater precision than the reported approximate energy consumption (up to 1 decimal place) values as seen in earlier.

Table 8.5: Comparison of simulated combined adjusted range using FR, PO, POIR and POTA

Torque-distribution strategy	Adjusted Combined Range
FR with regen	247.0 miles
PO with regen	263.5 miles
PO with ideal regenerative braking	262.0 miles
PO with torque assist regenerative braking	259.8 miles

Hence, the POIR strategy was chosen for the vehicle, because of a better combined adjusted range than POTA and also a safer and better driving experience.

Chapter 9

Discussion

The development of the Propulsion Supervisory Controller (PSC) for an independent axle all-wheel drive electric vehicle has been discussed. An overview of the functional features like power-moding and Electronic Transmission Range Selection (ETRS) is provided. This is followed by a discussion of the torque architecture feature, which is more related to the performance of the vehicle. The torque architecture includes the positive (forward) as well as the negative (regenerative) torque distribution logic, which has also been discussed at length. Functional and performance feature development is followed by software testing, HIL, sub-system and system integration. This is then followed by full vehicle testing, calibration and refinement. This study focuses more on the initial parts of propulsion controls development. This study also provides a brief overview of the vehicle architecture selection and PSC torque architecture logic. Based on comparison of different potential toque distribution logic, the penalized optimal strategy for positive torques combined with the ideal regenerative braking strategy for regenerative braking was found to be aligning with HEVT's goals going forward. During testing, the limits, derating and weights/penalty factors can be calibrated and refined for the modified vehicle over the testing and refinement phase. A simulated adjusted range of 262 miles was achieved using this strategy, which results in a simulated range improvement of 15 miles as compared to a simple fixed ratio strategy.

A plan going forward, is necessary to not only enable vehicle functionality, but systems safety (which is of foremost importance for HEVT) and meeting the vehicle technical spec-

ification goals set by the team. As sub-system level feature logic is implemented and integrated using a model-based approach, and verification is started, software verification and hardware-in-the-loop testing becomes important. As the development moves to sub-system and system integration, hardware-in-the-loop can help catch bugs in the Propulsion Controls software and communications early, which saves time. Once the system level integration and hardware-in-the-loop testing is completed, vehicle testing would be the next step. This would include completing a test-plan for the modified vehicle. Model validation of the modified model using a similar methodology as that discussed in this study would be crucial for calibration to improve the vehicle performance. A few other tasks in context of future scope as well as calibration and refinement would include:

Motor loss-maps: Improving the loss maps to better represent the specific drive units that the team has received (including HV bus voltage/SoC variation effect) would help improve the accuracy of the model. In general, the powertrain efficiency is higher for higher voltages, because of reduced I^2R losses. The HV battery voltage varies with battery SoC. The HV bus voltage would, hence, change as the SoC depletes during a drive-cycle, causing the powertrain efficiency to change as well. Further correction of the model would ensure more accurate evaluations.

Thermal derate strategy: Working with the drive unit manufacturers to create a more comprehensive thermal derate strategy would also be crucial from a systems safety standpoint. Currently, different temperatures are monitored for both drive units, like the coolant temperature, or motor temperature are monitored. It is important that the strategy is defined for a worst-case scenario, which means that all temperatures including the coolant temperature, stator and rotor temperatures, as well as the inverter temperatures are accounted for and the derating is conservative with regard to the relevant temperatures.

Accelerator Pedal map: Conducting testing to record the response of the vehicle to various accelerator pedal inputs at different speeds is necessary for calibrating the accelerator pedal

map. Ultimately, the goal would be to replicate and extend the base vehicle's pedal map and make the modified vehicle's pedal map comparable to that of the stock LYRIQ. Gear-backlash and drivability: During calibration, gear backlash and vehicle level jerk analysis would become important to make the vehicle's driving smoother. Modes like launch control, eco-driving etc. can be implemented. For drivability, the torque speed envelopes in the torque architecture of the PSC can be modified to ensure a smooth experience. This also ties into calibration of the pedal-map. Hill-hold: All the work in this study assumes a zero road slope. For cases where the vehicle is started facing up or down a slope, the torque architecture can be modified to detect the hill and hold the vehicle for giving the driver time to switch from a brake hold to the desired accelerator pedal input. One-pedal driving: This would require modification of the accelerator pedal map to blend negative/braking torques for accelerator pedal input below a certain threshold. This part also ties into the pedal map calibration.

Driving regimes: For this study, the UDDS and HWFET are used (to represent driving on city and highway respectively) to evaluate the energy consumption performance. Energy consumption evaluations for drive cycles like the US06 (high-speed aggressive driving), NEDC (New European Driving Cycle) or driving regimes specific to EcoCAR can be done. Road conditions: A factor that was constant in the current study was the road conditions. The road slope was a constant and the road adhesion parameters were also constant. How the energy consumption using the different torque distribution strategies would be affected by driving over different road types (for example driving on roads made from different materials such as asphalt, concrete, gravel, composite materials etc.) or conditions (like dry, wet, icy etc.) would also be important, considering that these are not constant in real-world driving. Lateral performance: The scope of this study has mostly been linear performance of the system, i.e., only in the longitudinal direction. But as the team gets close to the testing phase, ensuring that the torque architecture is safe with respect to lateral performance would be

critical for systems safety. The torque architecture for both positive torque (forward torque) and negative torque (regenerative braking torque) must not result in lateral instability. [6] states that control strategies can improve lateral performance, as well as energy consumption performance, in over-actuated vehicles. A control strategy to reduce oversteer and understeer effects during both forward acceleration and regenerative braking are discussed in [21]. A comparison of how the test vehicle in the study performs without control, with only motor control, and with motor control working alongside the electro-hydraulic brakes in the vehicle is discussed.

With regard to the blending between the friction and regenerative braking, it is crucial to maintain the energy efficiency, systems safety (with regard to lateral stability) and feel, as described in [17].In [18], a strategy to maximize regenerative braking has been developed, by developing a lookup-table based on a non-linear look-up table. As the vehicle drops speed, the drive-unit torque is derated to a point on the optimal line, based on the operating region, where the HV bus current switches direction. A similar approach can be used in the case of the current study, where the speed based derating factor can be further refined.

CSC integration: The CAVs supervisory controller transmits propulsion commands based on various sensor inputs. The PSC is then responsible for then, receiving these commands, arbitrating the commands, and transmitting the necessary signals. Integrating this logic is also important for CAVs features like eco-adaptive cruise control, automatic parking etc.

Chapter 10

Conclusions

The study summarizes the Propulsion Supervisory Controller (PSC) software development, and the model-based development approach used. A context of the architecture selection process has been provided. An overview of the vehicle model has also been provided. The model is then validated, and validation methodology is discussed. System safety is of utmost importance and some systems' safety features that are part of the torque architecture, like the thermal derate strategy, regenerative braking SoC and speed-based derating have also been discussed. An overview of the vehicle functionality features such as power moding and Electronic Transmission Range Selection has been provided. An analysis of vehicle performance for various torque distribution strategies is then presented. This evaluation is centered around the energy consumption performance of the vehicle, since energy efficiency is one of HEVT's priorities. Initially, torque distribution strategies exclusively for positive torques have been studied. The penalized optimal strategy (PO) reduces the simulated energy consumption over UDDS by 1 kWh/100 miles when compared to a simple fixed ratio strategy (FR), which translates to a 6.5 miles unadjusted range improvement. When regenerative braking is introduced, the penalized optimal strategy improves the vehicle's adjusted combined range by 16.5 miles as compared to a simple fixed ratio strategy. It is also observed that using regenerative braking improves the adjusted combined range by approximately 27% on an average, considering the PO and FR. The penalized optimal strategy for positive torques combined with the ideal regenerative braking strategy for regenerative braking

was found to be a reasonable balance, leaving room for calibration in context of drivability considerations for positive torques, as well as ensuring lateral stability during regenerative braking. Overall, the penalized optimal strategy for positive torques, with an ideal regenerative braking strategy, improves the simulated adjusted combined range of the vehicle by 15 miles as compared to the fixed ratio strategy. The study hence supports development of the torque architecture for the PSC of the independent axle dual drive-unit all-wheel drive electric vehicle that HEVT would be working on for the EcoCAR EV Challenge.

Bibliography

[1] Environmental Protection Agency (EPA). *2021 Test Car List Data*. 2021. URL: https://www.epa.gov/compliance-and-fuel-economy-data/data-cars-used-testing-fuel-economy.

[2] Environmental Protection Agency (EPA). *2023 Test Car List Data*. 2023. URL: https://www.epa.gov/compliance-and-fuel-economy-data/data-cars-used-testing-fuel-economy.

[3] *ABOUT THE ECOCAR EV CHALLENGE*. https://avtcseries.org/about-the-ecocar-ev-challenge/. Accessed: 2024-07-12. 2024-07-05.

[4] Feyijimi Adegbohun et al. "High Performance Electric Vehicle Powertrain Modeling, Simulation and Validation". In: *Energies* 14.5 (2021). ISSN: 1996-1073. DOI: 10.3390/en14051493. URL: https://www.mdpi.com/1996-1073/14/5/1493.

[5] George Baure and Matthieu Dubarry. "Synthetic vs. Real Driving Cycles: A Comparison of Electric Vehicle Battery Degradation". In: *Batteries* 5.2 (2019). ISSN: 2313-0105. DOI: 10.3390/batteries5020042. URL: https://www.mdpi.com/2313-0105/5/2/42.

[6] S. Bhat, M. Davari, and M. Nybacka. "Study on Energy Loss due to Cornering Resistance in Over-Actuated Vehicles using Optimal Control". In: *SAE International Journal of Vehicle Dynamics, Stability, and NVH* 1.2 (2017), pp. 263–269. DOI: 10.4271/2017-01-1568.

[7] R. Carlson et al. "The Measured Impact of Vehicle Mass on Road Load Forces and Energy Consumption for a BEV, HEV, and ICE Vehicle". In: *SAE International Jour-*

nal of Alternative Powertrains 2.1 (2013), pp. 105–114. DOI: 10.4271/2013-01-1457. URL: https://doi.org/10.4271/2013-01-1457.

[8] Renji V. Chacko, M. L. Sreedevi, and G. R. Mineeshma. "Electric vehicle power train simulation in forward modelling approach to enable real-time simulation and HIL controller prototyping". In: *2014 IEEE International Conference on Power Electronics, Drives and Energy Systems (PEDES)*. 2014, pp. 1–6. DOI: 10.1109/PEDES.2014.7042039.

[9] Yan Chen and Junmin Wang. "Design and Experimental Evaluations on Energy Efficient Control Allocation Methods for Overactuated Electric Vehicles: Longitudinal Motion Case". In: *Mechatronics, IEEE/ASME Transactions on* 19 (Apr. 2014), pp. 538–548. DOI: 10.1109/TMECH.2013.2249591.

[10] Federal Highway Administration. *Section 3: Benefits and Costs of Implementing SEITS*. Retrieved July 11, 2024, from https://ops.fhwa.dot.gov/publications/seitsguide/section3.htm. Accessed: 2024-07-11. n.d.

[11] Thomas Finken and Kay Hameyer. "Design of electric motors for hybrid-and electric-vehicle applications". In: *ICEMS*. 2009.

[12] Ford Motor Company. *2021 Ford Mustang Mach-E Technical Specifications*. Tech. rep. Accessed: 2022-11-21. Ford Motor Company, 2022.

[13] *Fortune Business insights*. https://www.fortunebusinessinsights.com/industry-reports/electric-vehicle-market-101678. Accessed: 2024-07-09. 2024-07-04.

[14] Yimin Gao, Liping Chen, and Mehrdad Ehsani. "Investigation of the Effectiveness of Regenerative Braking for EV and HEV". In: *SAE Transactions* 108 (1999), pp. 3184–3190. ISSN: 0096736X, 25771531. URL: http://www.jstor.org/stable/44733986 (visited on 08/07/2024).

[15] Cong Geng et al. “Simulation Research on Regenerative Braking Control Strategy of Hybrid Electric Vehicle”. In: *Energies* 14.8 (2021). ISSN: 1996-1073. DOI: 10.3390/en14082202. URL: https://www.mdpi.com/1996-1073/14/8/2202.

[16] Jingang Guo, Junping Wang, and Binggang Cao. “Regenerative braking strategy for electric vehicles”. In: *2009 IEEE Intelligent Vehicles Symposium*. 2009, pp. 864–868. DOI: 10.1109/IVS.2009.5164393.

[17] J. Hartley et al. “Braking System for a Full Electric Vehicle with Regenerative Braking”. In: *SAE Technical Paper*. 2010-01-1680. 2010. DOI: 10.4271/2010-01-1680. URL: https://doi.org/10.4271/2010-01-1680.

[18] Shoeib Heydari et al. “Optimal Blending of Regenerative and Friction Braking at Low Speeds for Maximizing Energy Extraction in Electric Vehicles”. In: *2019 IEEE Energy Conversion Congress and Exposition (ECCE)*. 2019, pp. 6815–6819. DOI: 10.1109/ECCE.2019.8913117.

[19] Hao Hu, Guoqing Xu, and Yang Zhu. “Hardware-In-the-Loop Simulation of Electric Vehicle Powertrain System”. In: *2009 Asia-Pacific Power and Energy Engineering Conference*. 2009, pp. 1–5. DOI: 10.1109/APPEEC.2009.4918397.

[20] Sopan Kane, Douglas Nelson, and Scott Huxtable. “Comparison of torque-split strategies for an independent axle, dual-motor all-wheel drive electric vehicle”. In: *2024 IEEE Transportation Electrification Conference and Expo (ITEC)*. 2024, pp. 1–5. DOI: 10.1109/ITEC60657.2024.10598925.

[21] Donghyun Kim, Sungho Hwang, and Hyunsoo Kim. “Rear motor control for a 4WD hybrid electric vehicle stability”. In: *IEEE International Conference on Vehicular Electronics and Safety, 2005.* 2005, pp. 86–91. DOI: 10.1109/ICVES.2005.1563619.

[22] K. Koprubasi et al. “Application of Model-Based Design Techniques for the Control Development and Optimization of a Hybrid-Electric Vehicle”. In: *SAE Technical Paper*. 2009-01-0143. 2009. DOI: 10.4271/2009-01-0143. URL: https://doi.org/10.4271/2009-01-0143.

[23] James Larminie and John Lowry. *Electric vehicle technology explained*. Wiley, 2012.

[24] Jinhao Liang et al. “A Hierarchical Control of Independently Driven Electric Vehicles Considering Handling Stability and Energy Conservation”. In: *IEEE Transactions on Intelligent Vehicles* 9.1 (2024), pp. 738–751. DOI: 10.1109/TIV.2023.3335251.

[25] D. Mackanic et al. “Development of a Software-In-The-Loop Model for a Parallel Plug-In Hybrid Electric Vehicle”. In: *SAE Technical Paper*. 2016-01-1255. 2016. DOI: 10.4271/2016-01-1255. URL: https://doi.org/10.4271/2016-01-1255.

[26] Yi Meng et al. “Test Correlation Framework for Hybrid Electric Vehicle System Model”. In: *SAE Int. J. Engines* 4.1 (2011), pp. 1046–1057. DOI: 10.4271/2011-01-0881. URL: https://doi.org/10.4271/2011-01-0881.

[27] Hoyong Na et al. “Optimal torque split strategies for dual motor EV”. In: ().

[28] Douglas Nelson. *Personal Communication*. Personal communication, 2023. 2023.

[29] Michael Panagiotidis, George Delagrammatikas, and Dennis Assanis. “Development and Use of a Regenerative Braking Model for a Parallel Hybrid Electric Vehicle”. In: *SAE Transactions* 109 (2000), pp. 1180–1191. ISSN: 0096736X, 25771531. (Visited on 09/15/2024).

[30] P. Phlips. “Analytic engine and transmission models for vehicle fuel consumption estimation”. In: *SAE International* 8.2 (2015), pp. 423–440. DOI: 10.4271/2015-01-0981.

[31] Q. Ren, D.A. Crolla, and A. Morris. "Effect of transmission design on Electric Vehicle (EV) performance". In: *2009 IEEE Vehicle Power and Propulsion Conference*. 2009, pp. 1260–1265. DOI: 10.1109/VPPC.2009.5289707.

[32] *THE GLOBAL ELECTRIC VEHICLE MARKET OVERVIEW IN 2024*. https://www.virta.global/global-electric-vehicle-market. Accessed: 2024-07-04. 2024-06-14.

[33] US Department of Transportation. *Systems Engineering for Intelligent Transportation Systems*. US Department of Transportation, 2007.

[34] *Virtual Vehicle Composer*. https://www.mathworks.com/help/vdynblks/ref/virtualvehiclecomposer-app.html. Accessed: 2024-07-09. 2023-12-01.

[35] B. Wang, D.L.S. Hung, J. Zhong, et al. "Energy Consumption Analysis of Different BEV Powertrain Topologies by Design Optimization". In: *Int.J Automot. Technol.* 19 (2018), pp. 907–914. DOI: 10.1007/s12239-018-0087-z. URL: https://doi.org/10.1007/s12239-018-0087-z.

[36] Zhenpo Wang et al. "Optimal Component Sizing of a Four-Wheel Independently-Actuated Electric Vehicle With a Real-Time Torque Distribution Strategy". In: *IEEE Access* 6 (2018), pp. 49523–49536. DOI: 10.1109/ACCESS.2018.2801564.

[37] J. Y. Wong. *Theory of Ground Vehicles*. 4th. John Wiley Sons, 2022.

[38] H. Wu et al. "Hybrid Electric Vehicle Powertrain Controller Development Using Hardware in the Loop Simulation". In: *SAE Technical Paper*. 2013. DOI: 10.4271/2013-01-0156. URL: https://doi.org/10.4271/2013-01-0156.

[39] X. D. Xue, K. W. E. Cheng, and N. C. Cheung. "Selection of eLECTRIC mOTOR dRIVES for electric vehicles". In: *2008 Australasian Universities Power Engineering Conference*. 2008, pp. 1–6.

[40] Bowen Yang et al. “Energy Management Strategy for Dual-Motor-Based Electric Vehicle Powertrain Using Nonlinear Model Predictive Control”. In: *2021 IEEE Transportation Electrification Conference Expo (ITEC)*. 2021, pp. 206–211. DOI: 10.1109/ITEC51675.2021.9490176.

[41] X. Yuan, J. Wang, and K. Colombage. “Torque distribution strategy for a front and rear wheel driven electric vehicle”. In: *6th IET International Conference on Power Electronics, Machines and Drives (PEMD 2012)*. 2012, pp. 1–6. DOI: 10.1049/cp.2012.0316.

[42] Wei Zhang et al. “Research on Regenerative Braking of Pure Electric Mining Dump Truck”. In: *World Electric Vehicle Journal* 10.2 (2019), p. 39. DOI: 10.3390/wevj10020039. URL: https://doi.org/10.3390/wevj10020039.